Integrator for general spin-*s* Gross-Pitaevskii systems

Mudit Jain [*], Mustafa A. Amin,[†] and Han Pu [‡]

Department of Physics and Astronomy, Rice University, Houston, Texas 77005, USA

We provide an algorithm, i-SPin 2, for evolving general spin-*s* Gross-Pitaevskii or nonlinear Schrödinger systems carrying a variety of interactions, where the $2s + 1$ components of the "spinor" field represent the different spin-multiplicity states. We consider many nonrelativistic interactions up to quartic order in the Schrödinger field (both short and long range, and spin-dependent and spin-independent interactions), including explicit spin-orbit couplings. The algorithm allows for spatially varying external and/or self-generated vector potentials that couple to the spin density of the field. Our work can be used for scenarios ranging from laboratory systems such as spinor Bose-Einstein condensates (BECs), to cosmological or astrophysical systems such as self-interacting bosonic dark matter. As examples, we provide results for two different setups of spin-1 BECs that employ a varying magnetic field and spin-orbit coupling, respectively, and also collisions of spin-1 solitons in dark matter. Our symplectic algorithm is second-order accurate in time, and is extensible to the known higher-order-accurate methods.

I. INTRODUCTION

Physical systems described by the Gross-Pitaevskii equation (GPE)/nonlinear Schrödinger equation (NLSE) are ubiquitous in many areas of physics, ranging from laboratory systems such as ultracold atomic Bose-Einstein condensates (BECs) [1], nonlinear optics [2–8], water waves [9–11], etc., to cosmological scenarios concerning the phenomenology of cold dark matter [12–25]. In the case of BECs in the laboratory, atoms are cooled and trapped using magnetic or optical traps. With magnetic traps the various hyperfine levels of the atoms are lost and the system can be described using one-component (scalar) GPE/NLSE. The use of optical traps, however, gives leverage over the different possible hyperfine levels, resulting in the so-called spinor BECs [26–28]. Such a system can be described by a multicomponent GPE/NLSE.[1] Depending upon the atomic species and the experimental setup, the different spin components can have many types of both short-ranged and long-ranged self-interactions (in addition to interactions with the external trapping potential and magnetic field). For instance, the long-ranged interaction could be mediated by the dipolar ($\sim 1/r^3$) interaction potential generated due to the spin density of the Schrödinger field. The short-ranged self-interaction can be both spin independent and spin dependent. The former is the density-density interaction of type $\sim \rho^2$ where ρ is the total number density of the multicomponent Schrödinger field. The latter can come in different varieties. One such spin-dependent interaction is the usual spin-spin interaction of type $\sim \mathcal{S} \cdot \mathcal{S}$, where $\mathcal{S}$ is the intrinsic spin density of the field. Another spin-dependent interaction is the spin-singlet interaction which characterizes collisions between two particle spin-singlet states. Besides such self-interactions, there are other possible interactions such as the spin-orbit interaction. So far, various higher spin condensates have been achieved in laboratory experiments. For instance, see Refs. [29,30] for spin-1/2, Refs. [26,31,32] for spin-1, Refs. [33–37] for spin-2, and Refs. [38,39] for spin-3 condensates. Owing to their spin (hyperfine) structure, such BEC systems are promising for interesting effects such as topological spin textures [40,41], quantum spin Hall effect and topological insulators [42–46], atomic lasers [47,48], etc. See Refs. [28,49,50] and references therein for detailed reviews on the physics of spinor condensates, and Ref. [51] and references therein for a review of numerical methods relevant to spinor condensates. Some more recent numerical works on spinor condensate can be found in Refs. [52–54]. Understanding the behavior of such higher spin systems from an analytical and computational standpoint is therefore highly desired. In the cosmological scenario, the GPE/NLSE is used to describe the cold dark matter field, and can contain both the density-density and spin-spin interactions (in the case of higher spin dark matter), besides the usual gravitational interactions. For instance, in the case of vector dark matter, both of these self-interactions are present in the effective low-energy regime (Higgs phase) of the Abelian Higgs model [25,55]. Even in the case of massive spin-2 or bigravity constructions [56–62], there are quartic self-interactions of the massive spin-2 degree of freedom [63], and can very well result in spin-spin interactions in the nonrelativistic low-energy effective theory (besides the density-density interactions). Also see Ref. [64] for a recent ghost-free massive spin-2 construction involving affine

---

*mudit.jain@rice.edu
†mustafa.a.amin@rice.edu
‡hpu@rice.edu

[1]Throughout this work, we generically refer to the hyperfine state, in the context of atomic, molecular, and optical (AMO) physics systems, as spin.

connections. Our work here, therefore, can naturally find its relevance in many cosmological and astrophysical scenarios. In this paper, we present a three-dimensional (3D) numerical algorithm involving the split Fourier technique, to evolve (a) *arbitrary spin-s* condensates containing both short- and long-ranged quartic self-interactions, in addition admitting (b) space- and time-dependent external vector fields $\bar{\boldsymbol{B}}(\boldsymbol{x}, t)$ [but separable such that $\bar{\boldsymbol{B}}(\boldsymbol{x}, t) = \boldsymbol{B}(\boldsymbol{x})f(t)$], leading to not only spatially and time-varying Zeeman effects, but also (and perhaps more importantly) giving rise to spin-orbit (SO) coupling. Last, we present (c) an explicit spin-orbit coupling term that couples the spin and the center-of-mass momentum. The SO coupling, arising in setups involving multiple lasers [30], and its effects have been gaining much interest recently [65,66]. This work can be contrasted with the existing literature, in which some work on this front already exists: In Ref. [67], a similar split Fourier technique was employed for spin-1 GPE containing both spin-spin and density-density short-ranged self-interactions, along with a spatially uniform linear and quadratic Zeeman term. In Ref. [68], the same situation was explored for a spin-2 system [69], with the addition of the spin-singlet interaction term. More recently, in Ref. [70] the authors presented a GPU-assisted approach to accelerate solving two-dimensional (2D) spin-1/2 GPE/NLSE. Our work in this paper differs from the existing literature in the three points listed in the previous paragraph. Also, contrary to a previous algorithm "i-SPin" laid out by some of us in Ref. [71] where the *n*-component Schrödinger field had an SO(*n*) symmetry, systems of consideration in this paper are describable by a $(2s + 1)$-component Schrödinger field, with components characterizing the different spin multiplicity states. Viewing the present algorithm in conjunction with this earlier work, we have called the present algorithm i-SPin 2. Our symplectic (unitary) algorithm employs the split-Fourier step technique in which the field evolution over a time step is broken into a half "drift" piece, followed by a "kick" piece, and then another half drift piece. In the drift pieces, the field is evolved using the drift Hamiltonian density that contains the usual Laplacian term together with the SO coupling term. In the kick piece, the field is evolved using the interaction Hamiltonian density which contains all of the rest of the interaction terms. By explicitly constructing the unitary evolution matrices in both the drift and the kick steps, we present a symplectic time-reversible algorithm. The accuracy of the field evolution in this algorithm is $O(\epsilon^2)$ (where ϵ is the time discretization step), which can be upgraded towards higher-order symplectic integrators that employ the split-step technique.

The paper is organized as follows. In Sec. II we begin by laying out the general (nonrelativistic) spin-*s* Schrödinger system containing all interactions of interest, including interactions with external scalar and vector fields. Then in Sec. III we work out the analytical solution for the field evolution due to both the drift and kick Hamiltonian densities, with the most nontrivial bit being the exponential of spin matrices. In Sec. 32 we present the general scheme of exponentiating arbitrary spin-*s* matrices, and provide explicit results for spin-1, spin-2, and spin-3 cases in Appendix B. With the analytical solution at hand, the general algorithm scheme is provided in Sec. 35. Our work has a broad domain of applicability, ranging from AMO physics in the laboratory to self-interacting fuzzy dark

matter in cosmology. We discuss this in Sec. 40, and present some simulation results for three example scenarios, demonstrating the effects of some of the interactions of interest. Section VII presents the summary of our work. In Appendix A we present the conventional forms for the spin matrices for spin-1 and spin-2 cases that are more suited for cosmology. In order to demonstrate the symplectic and reversible nature of our algorithm, in Appendix C, we provide the total number and spin conservation plots for our three example cases, together with a reversibility plot for the cosmology case.

Units and conventions. Throughout the paper and unless explicitly written, we work in natural units where $\hbar = 1 = c$. We also assume Einstein summation convention.

II. SPIN-*S* GROSS-PITAEVSKII/SCHRÖDINGER SYSTEM

A. Action and equation of motion

Our system comprises a $(2s + 1)$-component Schrödinger field $\Psi = (\psi_s, \psi_{s-1}, \dots, \psi_{-s})$ of mass μ, where different components represent the various spin multiplicity levels. More formally, Ψ transforms as a vector or "spinor" in the $(2s + 1)$-dimensional irreducible unitary representation of the SO(3) group.[2] For this system, we consider the following general action up to quartic order in the field Ψ, including all the relevant self-interactions (to leading order in the nonrelativistic limit):

$$\mathcal{S}_{\text{nr}} = \int dt \, d^3x \left[\frac{i}{2} \psi_n^\dagger \dot{\psi}_n + \text{c.c.} - \frac{1}{2\mu} \boldsymbol{\nabla} \psi_n^\dagger \cdot \boldsymbol{\nabla} \psi_n \right.$$
$$- \mu \rho V(\boldsymbol{x}) - \gamma \, \boldsymbol{\mathcal{S}} \cdot \bar{\boldsymbol{B}}(\boldsymbol{x}, t) - V_{\text{nrel}}(\rho, \boldsymbol{\mathcal{S}})$$
$$- \frac{\xi}{2} \frac{1}{(2s + 1)} |\psi_n \hat{A}_{nn'} \psi_{n'}|^2$$
$$\left. + i \, g_{ij} \, \psi_n^\dagger \, [\hat{S}_i]_{nn'} \, \boldsymbol{\nabla}_j \, \psi_{n'} \right], \quad (1)$$

with $\bar{\boldsymbol{B}}(\boldsymbol{x}, t) = f(t)\boldsymbol{B}(\boldsymbol{x})$, and

$$V_{\text{nrel}}(\rho, \boldsymbol{\mathcal{S}}) = -\frac{1}{2\mu^2}[\lambda \rho^2 + \alpha \, (\boldsymbol{\mathcal{S}} \cdot \boldsymbol{\mathcal{S}})]. \quad (2)$$

The first two terms in action (1) dictate the usual free field evolution (of each of the field components ψ_m, where $m \in [-s, s]$). The third and fourth terms account for interactions of the field with the external scalar trapping potential $V(\boldsymbol{x})$ and vector field $\bar{\boldsymbol{B}}(\boldsymbol{x}, t)$, coupling to the number density $\rho = \psi_n^\dagger \psi_n$ and spin density $\boldsymbol{\mathcal{S}} = \psi_n^* \hat{S}_{nn'} \psi_{n'}$, respectively.[3] Here

---

[2]The quotation marks around "spinor" are to highlight that it is not the fermion spinor that is usually referred to in the context of particle physics and quantum field theory. We will drop the quotes in the rest of the paper.

[3]Apart from the linear Zeeman term $\sim \psi^\dagger \, \boldsymbol{B} \cdot \boldsymbol{S} \, \psi$, there could also be a quadratic Zeeman term $\sim \psi^\dagger \, (\boldsymbol{B}' \cdot \hat{\boldsymbol{S}})^2 \, \psi$ which we do not consider explicitly. While it is trivial to include if $\boldsymbol{B}'$ is homogeneous, for the nonhomogeneous case it should also not be difficult to include, using the general spin matrix exponential scheme presented in Sec. 32 (applied towards exponentiation of the square of spin matrices).

$\hat{S}_x = \hat{x} \cdot \mathbf{\hat{S}}$ (and similarly for y and z) are the $[(2s + 1) \times (2s + 1)]$-dimensional spin matrices with the usual commutation relations

$$[\hat{S}_x, \hat{S}_y] = i\hat{S}_z \quad \text{with all cyclic permutations.} \tag{3}$$

The fifth term in action (1) accounts for quartic self-interactions of the Schrödinger field, which can depend on both number density and spin density [as seen in Eq. (3) explicitly]. The sixth term in Eq. (1) accounts for the two-body spin-singlet interaction, where the total spin multiplicity due to both the incoming and outgoing states adds to zero. The spin-singlet matrix is real and has the following properties:

$$\hat{A}^{-1} = \hat{A} = \hat{A}^T, \; \hat{A}\hat{S}_i\hat{A} = -\hat{S}_i^*, \; \psi^T \hat{A} \hat{S}_i \psi = 0, \tag{4}$$

and an explicit form for it is given ahead in Eq. (9). Finally, the last (seventh) term in Eq. (1) accounts for SO coupling where g_{ij} are real constants, with i and j being spatial indices. Specifically, $g_{ij} \propto \epsilon_{ij3}$ (the Levi-Città symbol) gives the well-known Rashba SO coupling, usually studied in the context of two-component BECs. Similarly, $g_{ij} \propto |\epsilon_{ij3}|$ gives the Dresselhaus SO coupling. Action (1) leads to the following equation of motion, the Schrödinger/Gross-Pitaevskii equation:

$$
\begin{aligned}
i\partial_t \psi_n = \Bigg[&\delta_{nn'}\left(-\frac{1}{2\mu}\mathbf{\nabla}^2\right) + \left(\mu V(\mathbf{x}) - \frac{\lambda}{\mu^2}\rho\right)\delta_{nn'} \\
&+ \gamma\, f(t)\mathbf{B}(\mathbf{x}) \cdot \mathbf{\hat{S}}_{nn'} \; - \; \frac{\alpha}{\mu^2}\mathbf{\mathcal{S}} \cdot \mathbf{\hat{S}}_{nn'} \\
&+ \frac{\xi}{2s+1}\hat{A}_{nm}\,\psi_m^*\psi_{m'}\,\hat{A}_{m'n'} \\
&- i\, g_{ij}\,[\hat{S}_i]_{nn'}\,\mathbf{\nabla}_j \Bigg]\psi_{n'}.
\end{aligned}
\tag{5}
$$

We break the Hamiltonian density (the term in the brackets above) into a drift and a kick piece as follows:

$$
\begin{aligned}
[\mathcal{H}_{\text{drift}}]_{nn'} &\equiv \delta_{nn'}\left(-\frac{1}{2\mu}\mathbf{\nabla}^2\right) - i\, g_{ij}\,[\hat{S}_i]_{nn'}\,\mathbf{\nabla}_j, \\
[\mathcal{H}_{\text{kick}}]_{nn'} &\equiv \left(\mu V(\mathbf{x}) - \frac{\lambda}{\mu^2}\rho\right)\delta_{nn'} + \gamma\, f(t)\mathbf{B}(\mathbf{x}) \cdot \mathbf{\hat{S}}_{nn'} \\
&\quad - \frac{\alpha}{\mu^2}\mathbf{\mathcal{S}} \cdot \mathbf{\hat{S}}_{nn'} + \frac{\xi}{2s+1}\hat{A}_{nm}\,\psi_m^*\psi_{m'}\,\hat{A}_{m'n'}.
\end{aligned}
\tag{6}
$$

Throughout this work, we work in the z basis. That is, the spin matrix $\hat{S}_z$ is diagonal, with the eigenvalues $m \in [-s, s]$ along the diagonal. Explicitly, and more suited for AMO systems, the spin matrices $\hat{S}_i$ and the spin-singlet matrix $\hat{A}$ take the following conventional forms, respectively:

$$[\hat{S}_x]_{nn'} = \frac{1}{2}(\delta_{n,n'+1} + \delta_{n+1,n'})\sqrt{s(s+1) - nn'},$$

$$[\hat{S}_y]_{nn'} = \frac{1}{2i}(\delta_{n,n'+1} - \delta_{n+1,n'})\sqrt{s(s+1) - nn'},$$

$$[\hat{S}_z]_{nn'} = \delta_{n,n'}\, n, \tag{7}$$

$$\hat{A}_{nn'} = (-1)^{s-n}\delta_{n,-n'}. \tag{8}$$

From a relativistic field theory or particle physics point of view, on the other hand (more suited for cosmology), the spin

matrices take different forms. See Appendix A for details, and Sec. VI B for a discussion of cosmological applications of our work.

Long-range self potentials. The external potentials V and $\mathbf{\bar{B}}$ can also be easily appended with self-generated ones, suitable for different applications. Explicitly for purposes in contemporary (ultra)light dark matter cosmology, $V(\mathbf{x}) \to \Phi(t, \mathbf{x})$, where $\Phi(t, \mathbf{x})$ is the Newtonian potential, given by the Poisson equation

$$\mathbf{\nabla}^2\Phi(t, \mathbf{x}) = 4\pi\mu G\rho(t, \mathbf{x}). \tag{9}$$

Similarly in the context of AMO systems where atomic dipolar interactions are present, $\mathbf{\bar{B}}(t, \mathbf{x}) \to \mathbf{\nabla}a(t, \mathbf{x})$, where a is a scalar field obeying the following Poisson equation:

$$\mathbf{\nabla}^2 a(t, \mathbf{x}) = \gamma\, \mathbf{\nabla} \cdot \mathbf{\mathcal{S}}(t, \mathbf{x}). \tag{10}$$

B. Conserved quantities and continuity equations

The only conserved quantity, associated with our nonrelativistic system (1), is the total particle number N (or equivalently the total mass $M = \mu N$):

$$N = \int d^3x\, \rho. \tag{11}$$

Furthermore, the local continuity equations for the number and spin densities are

$$
\begin{aligned}
\partial_t\rho + \mathbf{\nabla} \cdot \mathbf{\mathcal{J}}_{ll} &= 0, \\
\partial_t\mathbf{\mathcal{S}} + \mathbf{\hat{S}}_{nn'}(\mathbf{\nabla} \cdot \mathbf{\mathcal{J}}_{n'n}) &= (\gamma f\, \mathbf{B} \times \mathbf{\mathcal{S}}) + \mathbf{\mathcal{J}}',
\end{aligned}
\tag{12}
$$

respectively, where $\mathbf{\mathcal{J}}_{mn}$ is a general Schrödinger current matrix given by

$$\mathbf{\mathcal{J}}_{n'n} \equiv \frac{i}{2\mu}[\psi_{n'}\mathbf{\nabla}\psi_n^* - \psi_n^*\mathbf{\nabla}\psi_{n'}], \tag{13}$$

and $\mathbf{\mathcal{J}}'$ is the SO current term

$$\mathcal{J}_i' = i\, g_{kj}\,\epsilon_{k\ell i}\,\mathbf{\nabla}_j\mathcal{S}_\ell. \tag{14}$$

In the spin continuity equation, the first term on the right-hand side gives rise to the well-known spin precession effect, while the second term dictates the SO coupling effect. For the case when $\mathbf{\bar{B}}$ is time independent (meaning $f = $ const), the total energy in the system is also conserved. Furthermore, if $\mathbf{\bar{B}}$ and V are constants in both space and time and $g_{ij} = 0$, the total linear momentum and the parallel component of the total angular momentum (parallel to $\mathbf{\bar{B}}$) are also conserved (with orbital and spin angular momentum conserved separately). Also, the magnitudes of the total orbital and spin angular momentum are (separately) conserved. Adding the self-generated Newtonian potential or the dipolar potential does not change these results.

III. EVOLUTION OF THE SCHRÖDINGER FIELD

We employ a split Fourier algorithm in which the evolution of the Schrödinger field is broken into two parts: drift and kick as dictated by the respective Hamiltonian densities in Eqs. (7). In this section we present the general scheme of the Schrödinger field evolution for arbitrary integer spin fields, due to both the drift and kick Hamiltonian densities.

A. Evolution due to the drift Hamiltonian density

This evolution [cf. Eqs. (7)] is dictated by the following differential equation:

$$i\partial_t \psi_n = \left[\delta_{nn'}\left(-\frac{1}{2\mu}\nabla^2\right) - i\,g_{ij}\,[\hat{S}_i]_{nn'}\,\nabla_j \right]\psi_{n'}\,. \quad (15)$$

Evidently, the evolution is most easily performed in Fourier space. With $\tilde{\psi}(\boldsymbol{k})$ as the Fourier-transformed field (and $e^{i\boldsymbol{k}\cdot\boldsymbol{x}}$ as the forward Fourier coefficient), we have

$$i\partial_t \tilde{\psi}_n = \left[\delta_{nn'}\left(\frac{k^2}{2\mu}\right) - g_{ij}\,[\hat{S}_i]_{nn'}\,k_j \right]\tilde{\psi}_{n'}\,, \quad (16)$$

giving

$$\tilde{\psi}_n(t) = e^{-i(t-t_0)k^2/2\mu}[e^{i(t-t_0)g_{ij}k_j\hat{S}_i}]_{nn'}\tilde{\psi}_{n'}(t_0)\,. \quad (17)$$

Note that the order of the two exponentials here does not matter since the respective operations commute. Nevertheless, the most nontrivial task in the above is the matrix exponentiation, needed for the SO coupling term. We present matrix exponentials for the general spin-s case in Sec. 32 ahead.

B. Evolution due to the kick Hamiltonian density

Next comes the contribution from the kick Hamiltonian density [cf. Eqs. (7)], dictating the following differential evolution:

$$i\partial_t \psi_n = \left[\left(\mu V - \frac{\lambda}{\mu^2}\rho\right)\delta_{nn'} + \gamma\,f(t)\,\boldsymbol{B}\cdot\hat{\boldsymbol{S}}_{nn'} \right.$$
$$\left. - \frac{\alpha}{\mu^2}\,\boldsymbol{S}\cdot\hat{\boldsymbol{S}}_{nn'} + \frac{\xi}{2s+1}\hat{A}_{nm}\,\psi_m^*\psi_{m'}\,\hat{A}_{m'n'} \right]\psi_{n'}\,. \quad (18)$$

Here we have suppressed the explicit spatial dependence of V and $\boldsymbol{B}$ to be concise in our notation. To get the analytical solution to the above differential equation, we can handle the four different terms on the right-hand side in steps. For this purpose, it will be useful to define the following exponential

operators,

$$\hat{\mathcal{B}}_{nn'}(t,t_0) = [e^{-i\gamma\,F(t,t_0)\boldsymbol{B}\cdot\hat{S}}]_{nn'}\,,$$
$$\hat{\mathcal{G}}_{nn'}(t,t_0) = [e^{i(\alpha/\mu^2)(t-t_0)\boldsymbol{S}(t_0)\cdot\hat{S}}]_{nn'}\,, \quad (19)$$

where for ease of notation we have defined $F(t,t_0) \equiv \int_{t_0}^t \mathrm{d}\tau\,f(\tau)$, and explicitly state the property

$$[e^{ih(t)\,\boldsymbol{v}\cdot\hat{S}}]^T\,\hat{A}\,e^{ih(t)\,\boldsymbol{v}\cdot\hat{S}} = \hat{A}, \quad (20)$$

where $\boldsymbol{v}$ is any (time-independent) vector. The above can be seen to hold true on account of properties (6). To begin with, first note that the number density is constant throughout the kick evolution (19). This can be seen directly by recalling that there are no Schrödinger currents in the kick step [cf. Eq. (13) with $\mathcal{J} = 0$]. To account for the evolution due to $\boldsymbol{B}$, we plug the following ansatz,

$$\psi_n(t) = e^{-i(t-t_0)(\mu V - (\lambda/\mu^2)\rho)}\hat{\mathcal{B}}_{nn'}(t,t_0)\phi_{n'}(t), \quad (21)$$

into Eq. (19), to have the remaining evolution due to the spin-spin and spin-singlet self-interaction:

$$i\partial_t \phi_n = -\frac{\alpha}{\mu^2}\hat{\mathcal{B}}_{n\ell}^\dagger(t,t_0)\,[\boldsymbol{S}(t)\cdot\hat{S}]_{\ell m'}\,\hat{\mathcal{B}}_{m'n'}(t,t_0)\phi_{n'}$$
$$+ \frac{\xi}{2s+1}\hat{A}_{n\ell}\,\phi_{\ell'}^*\phi_\ell\,\hat{A}_{\ell n'}\phi_{n'}\,. \quad (22)$$

Here in the second line, we made use of properties (6), in order to simplify the term $[\hat{\mathcal{B}}^\dagger\hat{A}\hat{\mathcal{B}}^*]_{n\ell'} = -[\hat{\mathcal{B}}^\dagger\hat{\mathcal{B}}\hat{A}]_{n\ell'} = -\hat{A}_{n\ell'}$, and also $\hat{\mathcal{B}}_{m\ell}[\hat{A}\hat{\mathcal{B}}]_{mn'} = -[\hat{\mathcal{B}}^\dagger\hat{\mathcal{B}}]_{mn'}\hat{A}_{m\ell} = -\hat{A}_{n'\ell} = -\hat{A}_{\ell n'}$. Now, the matrix in the first term of Eq. (23) is nothing but the backwards evolution of the spin density $\boldsymbol{S}(t)$, giving the spin density at the initial instant, $\boldsymbol{S}(t_0)$. To see this, let us decompose $\boldsymbol{S}(t)$ and $\hat{\boldsymbol{S}}$ into parallel and perpendicular components, with respect to the external field $\boldsymbol{B}$. Owing to the spin precession during the kick step, dictated by the only nonzero (first) term on the right-hand side of the spin density continuity equation [cf. Eq. (13) with $\mathcal{J} = 0 = \mathcal{J}'$], the parallel spin density $\mathcal{S}_{||}$ does not change. However, the perpendicular components of the spin density do evolve. Decomposing these perpendicular components into raising and lowering pieces, $\mathcal{S}_+$ and $\mathcal{S}_-$ (using the usual convention of right-handed orientation[4]), we get the following:

$$\hat{\mathcal{B}}_{m\ell}^\dagger(t,t_0)\,[\boldsymbol{S}(t)\cdot\hat{S}]_{\ell n}\,\hat{\mathcal{B}}_{nm'}(t,t_0) = \left[\mathcal{S}_{||}(t_0)\hat{S}_{||} + \frac{1}{2}[e^{iB\hat{S}_{||}\,F(t,t_0)}][\mathcal{S}_-(t)\hat{S}_+ + \mathcal{S}_+(t)\hat{S}_-][e^{-iB\hat{S}_{||}\,F(t,t_0)}] \right]_{mm'}\,. \quad (23)$$

This can be simplified further. First note that the spin precession throughout the kick step, due to $\boldsymbol{B}$, goes as follows:

$$\mathcal{S}_+(t) = \mathcal{S}_+(t_0)\,e^{iBF(t,t_0)}\,,$$
$$\mathcal{S}_-(t) = \mathcal{S}_-(t_0)\,e^{-iBF(t,t_0)}\,. \quad (24)$$

------

[4]At any spatial location, calling the direction of $\boldsymbol{B}$ as x_3, the perpendicular spin matrices $\hat{S}_{x_1}$ and $\hat{S}_{x_2}$ can be used to define raising and lowering spin matrices as $\hat{S}_\pm \equiv \hat{S}_{x_1} \pm i\hat{S}_{x_2}$. Consecutively, we also define $\mathcal{S}_\pm \equiv \mathcal{S}_{x_1} \pm i\mathcal{S}_{x_2}$.

Upon using this together with the identity

$$[e^{iB\hat{S}_{||}\,F(t,t_0)}]\hat{S}_\pm[e^{-iB\hat{S}_{||}\,F(t,t_0)}] = \hat{S}_\pm\,e^{\pm iBF(t,t_0)} \quad (25)$$

in Eq. (23), the time dependence of the spin density drops out, giving

$$\hat{\mathcal{B}}_{m\ell}^\dagger(t,t_0)\,[\boldsymbol{S}(t)\cdot\hat{S}]_{\ell n}\,\hat{\mathcal{B}}_{nm'}(t,t_0) = [\boldsymbol{S}(t_0)\cdot\hat{S}]_{mm'}\,. \quad (26)$$

With this simplification, we now use the ansatz

$$\phi_n(t) = \hat{\mathcal{G}}_{nn'}(t,t_0)\,\chi_{n'}(t) \quad (27)$$

in Eq. (22) [appended by Eq. (26)] to give

$$i\partial_t \chi_n = \frac{\xi}{2s+1} \hat{A}_{n\ell'} \chi^*_{\ell'} \chi_\ell \hat{A}_{\ell n'} \chi_{n'}. \qquad (28)$$

Here once again, we have used properties (6) to simplify the terms $[\hat{\mathcal{G}}^\dagger \hat{A} \hat{\mathcal{G}}^*]_{n\ell'} = -[\hat{\mathcal{G}}^\dagger \hat{\mathcal{G}} \hat{A}]_{n\ell'} = -\hat{A}_{n\ell'}$, and $\hat{\mathcal{G}}_{m\ell}[\hat{A}\,\hat{\mathcal{G}}]_{mn'} = -[\hat{\mathcal{G}}^\dagger \hat{\mathcal{G}}]_{mn'} \hat{A}_{m\ell} = -\hat{A}_{n'\ell} = -\hat{A}_{\ell n'}$. From the above equation for χ, one can first obtain the evolution equation for the quantity $q \equiv \chi^T \hat{A} \chi = \psi^T \hat{A} \psi$. [The second equality holds true on account of property (23).] It simply rotates as a phasor: $q(t) = q(t_0)e^{-2i(t-t_0)\xi\rho/(2s+1)}$. With this, the ansatz $\chi(t) = \eta(t)e^{-i(t-t_0)\xi\rho/(2s+1)}$ can be used to get the following equation for η:

$$i\partial_t \eta_n = \frac{\xi}{2s+1}(q(t_0)\hat{A}_{n\ell'}\eta^*_{\ell'} - \rho\,\eta_n). \qquad (29)$$

This has the solution[5]

$$\eta_n(t) = \hat{\mathcal{U}}'_{n\ell}(t, t_0)\psi_\ell(t_0), \qquad (30)$$

where the operator $\hat{\mathcal{U}}'$ is given in Eq. (32) ahead [with the initial condition $\eta_n(t_0) = \psi_n(t_0)$]. In summary, combining all of the above pieces together, the full kick evolution becomes

$$\psi_m(t) = \hat{\mathcal{U}}_{mn}(t-t_0)\hat{\mathcal{U}}'_{n\ell}(t-t_0)\,\psi_\ell(t_0), \quad \text{where}$$

$$\hat{\mathcal{U}}_{mn}(t-t_0) = e^{-i(t-t_0)\left(\mu V - \left(\frac{\lambda}{\mu^2} - \frac{\xi}{(2s+1)}\right)\rho\right)}$$

$$\times \hat{\mathcal{B}}_{m\ell}(t, t_0)\,\hat{\mathcal{G}}_{\ell n}(t, t_0),$$

$$\hat{\mathcal{U}}'_{n\ell}(t, t_0) = \left[\cos\left(\frac{\xi\rho_q}{2s+1}(t-t_0)\right)\delta_{n\ell}\right.$$

$$+ \frac{i}{\rho_q}\sin\left(\frac{\xi\rho_q}{2s+1}(t-t_0)\right)$$

$$\left.\times (\rho\,\delta_{n\ell} - \hat{A}_{nn'}\psi^*_{n'}(t_0)\psi_{\ell'}(t_0)\hat{A}_{\ell'\ell})\right], \quad (31)$$

and where $\hat{\mathcal{B}}$ and $\hat{\mathcal{G}}$ are defined in Eq. (19), and $\rho_q \equiv \sqrt{\rho^2 - |q(t_0)|^2} = \sqrt{\rho^2 - |\psi_n(t_0)\hat{A}_{nm}\psi_m(t_0)|^2}$. This is our main equation for the evolution of the field ψ under the kick Hamiltonian density. It is important to note the order of the exponentials $\hat{\mathcal{B}}(t, t_0) = e^{-i\gamma\,\boldsymbol{B}\cdot\hat{\boldsymbol{S}}F(t,t_0)}$ and $\hat{\mathcal{G}}(t, t_0) = e^{i(\alpha/\mu^2)(t-t_0)\boldsymbol{\mathcal{S}}(t_0)\cdot\hat{\boldsymbol{S}}}$ in the above evolution equation. Unless $\boldsymbol{B}$ and $\boldsymbol{\mathcal{S}}$ are parallel, reversing the order leads to incorrect evolution since $\boldsymbol{B}\cdot\hat{\boldsymbol{S}}$ and $\boldsymbol{\mathcal{S}}\cdot\hat{\boldsymbol{S}}$ do not commute in general.

With the exact evolution for both the drift and the kick steps, Eqs. (17) and (31), respectively, we now require the analytical form for the matrix exponential $e^{-i\beta\,\boldsymbol{n}\cdot\hat{\boldsymbol{S}}}$ for a general spin-s system. Here $\boldsymbol{\beta} = \beta\boldsymbol{n}$ could be any function of $\boldsymbol{k}$ or $\boldsymbol{x}$ (relevant for SO drift and kick terms, respectively). For the SO term in the drift evolution, $\beta n_i = -(t - t_0)g_{ij}k_j$, while for the magnetic field coupling and spin-spin interaction in

the kick evolution, we have $\beta n_i = \gamma F(t, t_0)B_i$ and $\beta n_i = -(\alpha/\mu^2)(t-t_0)\mathcal{S}_i$, respectively. We pursue the relevant exercise in the next section.

IV. MATRIX EXPONENTIAL FOR GENERAL SPIN S

For any arbitrary spin s, the matrix exponential in general must take the following form:

$$e^{-i\beta\,\hat{\boldsymbol{n}}\cdot\hat{\boldsymbol{S}}} = \mathbb{I} + i\sum_{\ell=1}^{s}(\hat{\boldsymbol{n}}\cdot\hat{\boldsymbol{S}})^{2\ell-1}\left[\sum_{m=1}^{s}a_{m\ell}\sin m\beta\right]$$

$$+ \sum_{\ell=1}^{s}(\hat{\boldsymbol{n}}\cdot\hat{\boldsymbol{S}})^{2\ell}\left[\sum_{m=0}^{s}b_{m\ell}\cos m\beta\right]. \qquad (32)$$

Here $a_{m\ell}$ and $b_{m\ell}$ are real coefficients and $\mathbb{I}$ the $(2s+1)$-dimensional identity matrix. The reason that the above form must hold is threefold: (1) the conjugate transpose of the exponential must be the same as $\beta \to -\beta$; (2) all possible frequencies, $m \in [0, s]$, must appear in the expansion; and (3) the maximum power required of the matrix $(\hat{\boldsymbol{n}}\cdot\hat{\boldsymbol{S}})$ is $2s$, since all higher powers of this matrix can be written as linear combinations of $\mathbb{I}$, $(\hat{\boldsymbol{n}}\cdot\hat{\boldsymbol{S}})$, $(\hat{\boldsymbol{n}}\cdot\hat{\boldsymbol{S}})^2$, and so on up to $(\hat{\boldsymbol{n}}\cdot\hat{\boldsymbol{S}})^{2s}$ by virtue of the Cayley-Hamilton theorem. With the above form, the explicit values of the s^2 number of $a_{m\ell}$ and $s(s+1)$ number of $b_{m\ell}$ can be determined by matching the Taylor expansion of the exponential in β (only up to β^{2s}) on the left-hand side, with the similar Taylor expansion of the series form in the right-hand side of Eq. (32). For this matching purpose, it is easiest to work with $\hat{\boldsymbol{n}} = \hat{\boldsymbol{z}}$, since in our working z basis $\hat{S}_z$ is diagonal and equal to the last expression in Eq. (7). Upon performing this matching exercise, we get

$$\sum_{\ell=1}^{s}p^{2(\ell-r-1)}\left[\sum_{m=1}^{s}a_{m\ell}m^{2r+1}\right] = -1 \;\forall\; p = \{1, \ldots, s\}$$

$$\text{and}\;\; r = \{0, 1, \ldots, s-1\} \qquad (33)$$

from the odd terms in β (i.e., from the sine terms), while

$$\sum_{\ell=1}^{s}p^{2\ell}\left[\sum_{m=0}^{s}b_{m\ell}\right] = 0 \;\forall\; p = \{1, \ldots, s\},$$

$$\text{and}\;\; \sum_{\ell=1}^{s}p^{2(\ell-r)}\left[\sum_{m=0}^{s}b_{m\ell}m^{2r}\right] = 1$$

$$\forall\; p = \{1, \ldots, s\} \;\; \text{and}\;\; r = \{1, \ldots, s\} \qquad (34)$$

from the even terms in β (i.e., from the cosine terms). The above two sets of linear equations can be solved separately to get the coefficients a and b for an arbitrary spin-s system. We note that our results are consistent with the previous work on this subject [72–74]. In Appendix B we provide explicit expressions for spin-1, spin-2, and spin-3 systems.

V. ALGORITHM

A. Algorithm summary

Equipped with the analytical solution for both the drift and kick evolution along with arbitrary spin matrix exponential, the full split-step Fourier algorithm proceeds as follows. Starting with the field components $\psi_m(\boldsymbol{x}, t)$ at time t, they are

---

[5]The solution can be obtained by noting that $\ddot{\eta}_m = -\omega^2\eta_m$, where $\omega = (\xi/2s+1)\sqrt{\rho^2 - |q(t_0)|^2}$, which together with the initial conditions $\eta_m(t_0) = \psi_m(t_0)$ and $\dot{\eta}_m(t_0) = -(i\xi/(2s+1))(q(t_0)\hat{A}_{m\ell'}\psi^*_{\ell'}(t_0) - \rho\psi_m(t_0))$ [cf. Eq. (32)] gives the final solution of Eq. (30) See Ref. [68] for the same analysis.

drifted through a time step $\epsilon/2$ according to

$$i\partial_t \psi_n = \left[\delta_{nn'} \left(-\frac{1}{2\mu} \nabla^2 \right) - i\, g_{ij} \, [\hat{S}_i]_{nn'} \, \nabla_j \right] \psi_{n'}$$

$$\Rightarrow \psi_n^{(1)}(\boldsymbol{x}) = \int_{\boldsymbol{k}} \mathcal{F}_{\boldsymbol{k},\boldsymbol{x}}^{-1} \, e^{-i\epsilon\, \boldsymbol{k}^2/4\mu} [e^{i\epsilon\, g_{ij}k_j\hat{S}_i/2}]_{nn'}$$

$$\times \int_{\boldsymbol{w}} \mathcal{F}_{\boldsymbol{k},\boldsymbol{w}} \psi_{n'}(\boldsymbol{w},t) \,. \tag{35}$$

Here the symbol $\mathcal{F}$ represents Fourier transformation: $\int_{\boldsymbol{w}} \mathcal{F}_{\boldsymbol{k},\boldsymbol{w}} h(\boldsymbol{w},t) = \int \mathrm{d}^3 w \, e^{i\boldsymbol{k}\cdot\boldsymbol{w}} h(\boldsymbol{w},t) = h_{\boldsymbol{k}}(t)$. Similarly $\mathcal{F}^{-1}$ represents inverse Fourier transformation: $\int_{\boldsymbol{k}} \mathcal{F}_{\boldsymbol{k},\boldsymbol{x}}^{-1} h_{\boldsymbol{k}}(t) = \int \frac{\mathrm{d}^3 k}{(2\pi)^3} \, e^{-i\boldsymbol{k}\cdot\boldsymbol{x}} h_{\boldsymbol{k}}(t) = h(\boldsymbol{x},t)$.[6]

Then, every component is kicked through a time step ϵ according to

$$i\partial_t \psi_n = \left(\mu V - \frac{\lambda}{\mu^2}\rho \right) \psi_n + \gamma\, f(t)\, \boldsymbol{B}\cdot\hat{\boldsymbol{S}}_{nn'} \psi_{n'}$$

$$- \frac{\alpha}{\mu^2} \boldsymbol{\mathcal{S}}\cdot\hat{\boldsymbol{S}}_{nn'} \psi_{n'} + \frac{\xi}{2s+1} \hat{A}_{nm}\, \psi_m^*\, \psi_{m'}\, \hat{A}_{m'n'} \,,$$

$$\Rightarrow \psi_n^{(2)}(\boldsymbol{x}) = \hat{\mathcal{U}}_{n\ell}(\epsilon)\, \hat{\mathcal{U}}'_{\ell n'}(\epsilon)\, \psi_{n'}^{(1)}(\boldsymbol{x}) \,, \tag{36}$$

where the operators $\hat{\mathcal{U}}_{mn}(\epsilon)$ and $\hat{\mathcal{U}}'_{mn}(\epsilon)$ are given by Eqs. (31), with ρ, $\boldsymbol{\mathcal{S}}$, and ρ_q computed using $\boldsymbol{\Psi}^{(1)}$. In the case where V and $f\boldsymbol{B}$ are self-generated potentials [cf. Eq. (9) for self-gravity in the cosmological context, and Eq. (10) for self-dipolar field in the condensed matter context], they are easily computed in Fourier space as[7]

$$V \to \Phi(\boldsymbol{x}) = -4\pi\mu G \int_{\boldsymbol{k}} \mathcal{F}_{\boldsymbol{k},\boldsymbol{x}}^{-1} \frac{1}{k^2} \int_{\boldsymbol{w}} \mathcal{F}_{\boldsymbol{k},\boldsymbol{w}} \rho(\boldsymbol{w}) \,,$$

$$f\boldsymbol{B} \to \nabla a(\boldsymbol{x}) = -\gamma \int_{\boldsymbol{k}} \mathcal{F}_{\boldsymbol{k},\boldsymbol{x}}^{-1} \frac{\boldsymbol{k}}{k^2} \left[\boldsymbol{k}\cdot\int_{\boldsymbol{w}} \mathcal{F}_{\boldsymbol{k},\boldsymbol{w}} \boldsymbol{\mathcal{S}}(\boldsymbol{w}) \right]. \tag{37}$$

Finally, the fields are again drifted through a time step $\epsilon/2$:

$$i\partial_t \psi_n = \left[\delta_{nn'} \left(-\frac{1}{2\mu} \nabla^2 \right) - i\, g_{ij}\, [\hat{S}_i]_{nn'}\, \nabla_j \right] \psi_{n'} \Rightarrow \psi_n(\boldsymbol{x}, t+\epsilon)$$

$$= \int_{\boldsymbol{k}} \mathcal{F}_{\boldsymbol{k},\boldsymbol{x}}^{-1} \, e^{-i\epsilon\, \boldsymbol{k}^2/4\mu} [e^{i\epsilon\, g_{ij}k_j\hat{S}_i/2}]_{nn'} \int_{\boldsymbol{w}} \mathcal{F}_{\boldsymbol{k},\boldsymbol{w}} \psi_{n'}^{(2)}(\boldsymbol{w}) \,. \tag{38}$$

---

[6]In practice, we work with a Cartesian cubic grid with spatial resolution Δx in each direction, with a finite volume $V = (N\Delta x)^3 = L^3$. This leads to $\int_{\boldsymbol{k}} \to V^{-1}\sum_{\boldsymbol{k}}$ with $\boldsymbol{k} = 2(\Delta x)^{-1}\sin(\pi\boldsymbol{n}/N)$, and $\delta^{(3)}(\boldsymbol{x}-\boldsymbol{y}) \to V\delta_{\boldsymbol{x},\boldsymbol{y}}$. Here the sine function is used to account for the fact that the eigenvalues of the discrete difference operator in any ith direction is $4(\Delta x)^{-2}\sin^2(\pi n_i/N)$. As long as the field dynamics do not depend upon very high $\boldsymbol{k}$ modes on the lattice, which is anyways a necessity for trustworthy evolution of any system on the lattice, an equivalent definition of $\boldsymbol{k} = 2\pi\boldsymbol{n}/L$ suffices as well. (Note that the two definitions of $\boldsymbol{k}$ converge to one another for $|\boldsymbol{n}| \ll N$.)

[7]In these computations, we always discard the zero momentum mode for practical purposes. While we never encounter any inconsistencies or problems due to the exclusion of the $\boldsymbol{k} = 0$ mode, it can be nonetheless incorporated by employing different techniques. See, for example, Refs. [75–77].

The half-drift steps in the set of operations ensure $O(\epsilon^2)$ accuracy, while successive computation of the kick ensures reversibility. Since every operation is unitary, the full drift-kick-drift algorithm is symplectic and conserves total particle number. For cases with time-independent external potentials, the total spin is also conserved.

The relevant matrix exponentials appearing in both the kick and drift steps, for a general spin-s system, are obtained as in Eq. (32), augmented with Eqs. (33) and (34) to get the expansion coefficients. As examples, explicit expressions for spin 1, spin 2, and spin 3 are given in Appendix B. Relevant for cosmology and/or field theory, explicit expressions for spin-1 and spin-2 matrices are given in Appendix A.

B. Courant-Friedrichs-Lewy condition

In order to get a reliable field evolution, it must be ensured that the fastest process occurring in the system is sufficiently resolved. The Courant-Friedrichs-Lewy (CFL) condition takes care of this by choosing a sufficiently small time step ϵ. In the drift step there are two processes. One is the usual free field evolution (due to the Laplacian term) $\sim e^{i(\epsilon/2\mu)\nabla^2/2}$, and another is the SO term $\sim e^{i(\epsilon/2)gs|\nabla|}$, where we have replaced the spin matrix by s (for the maximum spin multiplicity corresponding to the fastest frequency) and g is the largest entry in the matrix g_{ij}. On the other hand, the kick evolution involves five different pieces. Two of them are due to couplings with external (or self-generated long-ranged) scalar and vector fields, giving $\sim e^{-i\epsilon\mu V}$ and $\sim e^{-i\epsilon\gamma Bfs}$, respectively. The other three are due to short-range self-interactions of the Schrödinger field. These give the factors $\sim e^{i\epsilon(\lambda/\mu^2)\rho}$ and $\sim e^{i\epsilon(\alpha/\mu^2)s\mathcal{S}}$ for density-density and spin-spin interactions, respectively, and $\sim e^{\pm i\epsilon\xi\rho_q/(2s+1)}$ for the spin-singlet interaction. Here recall that $\rho_q = \sqrt{\rho^2 - |q|^2}$ with $q = \psi^T A\psi$, and once again we have replaced the spin matrix in the exponent with the largest multiplicity (eigen) value s. With all these six different pieces, the CFL condition reads

$$\epsilon = 2\pi\,\delta\,\min\left[\frac{\mu}{3}(\Delta x)^2 , \frac{\Delta x}{\sqrt{3}\,s\,\max[g]} , |\mu V|^{-1} , |\gamma s f\boldsymbol{B}|^{-1} \right.$$

$$\left. \times \left| \frac{\lambda}{\mu^2}\rho \right|^{-1} , \left| \frac{\alpha}{\mu^2}s\boldsymbol{\mathcal{S}} \right|^{-1} , \left| \frac{\xi}{2s+1}\rho_q \right|^{-1} \right]. \tag{39}$$

Here $\delta \ll 1$ is a tuning parameter that dictates the amount by which the fastest oscillation is sampled. In the above, we have replaced ∇^2 by its value on the discrete lattice, $\sum_{i=1}^3 (\Delta x)^{-2} \times 4\sin^2(n_i\pi/N)$, and set $n = N/2$ along with $\sum \to 3$ in order to maximize the sum over sine functions. For the demonstration of the fidelity of the algorithm, we pick $\delta < 1/8$ and Δx small enough so that $\min[\cdots] = \mu(\Delta x)^2/3$ throughout the duration of the simulation.

VI. SCOPE AND APPLICATIONS

Here we discuss some of the applications of our system (1) in a variety of different contexts. In order to demonstrate the fidelity of our construction and scope of validity, we present

some simulation results on both the cold-atom and cosmology fronts.

A. Spinor quantum gases

In a quantum system, the interplay between the spin degrees of freedom and the spatial degrees of freedom often leads to a variety of intriguing phenomena. Spinor quantum gases represent an ideal platform to study such phenomena and, indeed, they have been at the forefront of cold-atom research in the past few decades. Here we will consider two specific examples related to spinor BECs. In the first example, the spinor BEC is subjected to an artificial monopole magnetic field and confined in a shell trapping potential; in the second, we consider an untrapped spinor BEC stabilized by the combination of self-attraction and the spin-orbit coupling. In both of these cases, we will present specific ground states of the systems, by performing imaginary time evolution.

1. Trapped spinor BECs in an effective magnetic monopole

We first consider the scenario outlined in Ref. [78]. Atoms with hyperfine spin s are subject to a spherically symmetric harmonic trap, together with a strong bias magnetic field $B_0 \hat{z}$ and a periodic quadruple magnetic field $B_1(1 - 4\tilde{\lambda} \cos \omega t)[x\hat{x} + y\hat{y} - 2z\hat{z}]$. The Zeeman effects due to the bias field can be removed by transforming into the rotating frame along the z axis (rotation frequency being equal to the Larmor frequency ω_L). Then, if $\omega = \omega_L$ and $\tilde{\lambda} = 1$, the magnetic field in the rotating frame has a time-independent piece that is radially outward, mimicking a monopole field, and a fast oscillating piece (with oscillating frequency $\omega = \omega_L$) that can be neglected. The effective Hamiltonian density in the rotating frame (including self-interactions) turns out to be

$$\mathcal{H} = \frac{1}{2\mu} \boldsymbol{\nabla} \psi_n^{\dagger} \cdot \boldsymbol{\nabla} \psi_n + \mu \, \rho \, V(\boldsymbol{r}) + \gamma \, \boldsymbol{\mathcal{S}} \cdot \boldsymbol{B}(\boldsymbol{r})$$
$$- \frac{1}{2\mu^2} [\lambda \rho^2 + \alpha \, (\boldsymbol{\mathcal{S}} \cdot \boldsymbol{\mathcal{S}})], \qquad (40)$$

leading to the following spinor Schrödinger equation:

$$i\partial_t \psi_n = \left[\delta_{nn'} \left(-\frac{1}{2\mu} \boldsymbol{\nabla}^2 \right) + \left(\mu \, V - \frac{\lambda}{\mu^2} \, \rho \right) \delta_{nn'} \right.$$
$$\left. + \gamma \boldsymbol{B} \cdot \hat{\boldsymbol{S}}_{nn'} - \frac{\alpha}{\mu^2} \boldsymbol{\mathcal{S}} \cdot \hat{\boldsymbol{S}}_{nn'} \right] \psi_{n'}. \qquad (41)$$

Here $V(\boldsymbol{r}) = \omega_T^2 \, r^2 / 2$, $\boldsymbol{B} = r \, \hat{\boldsymbol{r}}$, and $\gamma = 2\mu_B g_F B_1$ (where ω_T is the harmonic trap frequency, g_F is the Landé factor, and μ_B is the Bohr magneton). Owing to the Zeeman coupling of spin density $\boldsymbol{\mathcal{S}}$ with $\boldsymbol{B}$, we consider configurations where the local spin vectors are polarized opposite to the $\boldsymbol{B}$ field. That is, the spinor state is an eigenfunction of the spin operator along the radial direction, and with eigenvalues $m \in [-s, 0]$. The full Schrödinger field thus takes the following form:

$$\boldsymbol{\Psi}(\boldsymbol{r}, t) = \phi(\boldsymbol{r}, t) \, \mathcal{M}(\theta, \varphi) \boldsymbol{\chi}^{(m)}, \qquad (42)$$

where $\boldsymbol{\chi}^{(m)}$ is the eigenstate of the $\hat{S}_z$ operator with eigenvalue m, and $\mathcal{M}(\theta, \varphi) = e^{-i\varphi \hat{S}_z} e^{-i\theta \hat{S}_y}$ is the unitary transformation

matrix that rotates $\boldsymbol{\chi}^{(m)}$ to "point" along the radial direction.[8] With the above ansatz, the effective equation for the scalar field ϕ takes the following form[9]:

$$i\partial_t \phi = -\frac{1}{2\mu} \left(\boldsymbol{\nabla} - im \frac{\cot \theta}{r} \hat{\boldsymbol{\varphi}} \right)^2 \phi$$
$$+ \left(\frac{1}{2} \mu \omega_T^2 r^2 + \gamma m r + \frac{(s(s+1) - m^2)}{2\mu \, r^2} \right) \phi$$
$$- \frac{1}{\mu^2} \rho(\lambda + \alpha m |m|) \phi. \qquad (43)$$

Ignoring self-interactions for the moment, this dictates the motion of a scalar particle of "electric charge" m, in the background of a scalar potential equal to the second term in the first line, and a magnetic monopole at the center [cf. the vector gauge potential $\boldsymbol{A}(\boldsymbol{r}) = (\cot \theta / r) \hat{\boldsymbol{\varphi}}$]. To demonstrate our algorithm, we present the ground state of the above system for the spin-1 case and $m = -1$, with $\gamma = 4(\mu \omega_T^3)^{1/2}$. For this purpose, we worked in units where $\mu = \omega_T = 1$, and evolved the Euclidized Schrödinger equation, i.e., $t \to -i\tau$ in Eq. (41), beginning with an arbitrary Gaussian ansatz for ϕ [cf. Eq. (42)].[10] With the convergence criterion being

$$\frac{|\int d^3 x (\boldsymbol{\Psi}(\boldsymbol{x}, t + \epsilon) - \boldsymbol{\Psi}(\boldsymbol{x}, t))|}{|\int d^3 x \, \boldsymbol{\Psi}(\boldsymbol{x}, t)|} < 0.01, \qquad (44)$$

we found convergence towards the ground state shown in Fig. 1 around $t \sim 6$ (with the time step being $\epsilon \approx 0.06$). The presence of a cylindrical hole along the z axis is reflective of the gauge potential $\boldsymbol{A}$ in the effective system for ϕ, and can be thought of as a Dirac string. To validate the stationarity and robustness of the obtained ground state, we evolved it in real time and saw no variation (apart from the overall phase rotation). Furthermore, due to the symplectic nature of our algorithm, total mass and spin are conserved up to machine precision. The associated plots are presented in Appendix C. If $\gamma \gg (\mu \omega_T^3)^{1/2} (s(s+1) - m^2)^{1/4} (2m^4)^{-1/4}$, the minima of the scalar potential lies at $r_0 \simeq -\gamma m / (\mu \omega_T^2)$ (with $m < 0$), and the spinor field is expected to be tightly concentrated within the spherical shell at this radius. The problem reduces to that of a charged particle confined on a spherical surface subject to a magnetic monopole of charge m, centered at the origin [78].

---

[8] In our z working basis, $\boldsymbol{\chi}^{(m)}$ is a column vector with unity at the mth position, rest zero, meaning it is the mth column of the matrix $\mathcal{M}$.

[9] Here we used the identity $[e^{i\alpha \hat{S}_y}] \hat{S}_z [e^{-i\alpha \hat{S}_y}] = \hat{S}_z \cos \alpha - \hat{S}_x \sin \alpha$ (true for all cyclic permutations as well), along with $\sum_i \hat{S}_i^2 |\chi\rangle = s(s+1)|\chi\rangle$ and $\langle \chi | \hat{S}_{x,y} | \chi \rangle = 0$, to simplify expressions. We also inserted the relationship $\boldsymbol{\mathcal{S}} = |\phi|^2 \langle \chi | \mathcal{M}^{\dagger} \hat{S} \mathcal{M} | \chi \rangle = m |\phi|^2 \hat{\boldsymbol{r}}$. Finally, it is obvious that $\rho = \boldsymbol{\Psi}^{\dagger} \boldsymbol{\Psi} = |\phi|^2$.

[10] It is to be noted that in the imaginary time evolution, the total "wavefunction" must be renormalized at every time iteration; otherwise the total particle number dies out exponentially like $e^{-E_0 \tau}$, where E_0 is the ground state energy.
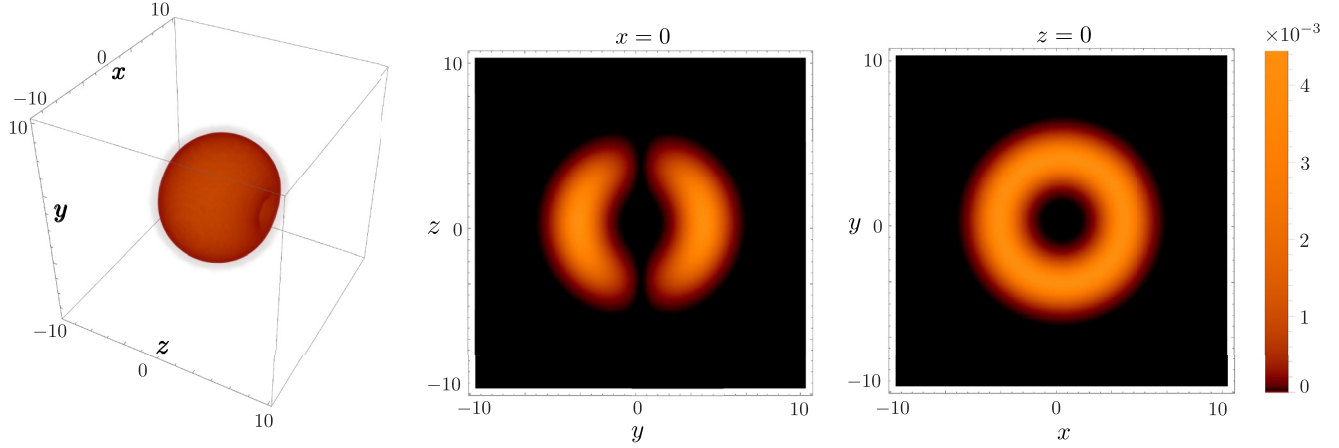
FIG. 1. A stationary state of the Hamiltonian density (41) with $\lambda = \alpha = 0$, for a spin-1 system with $m = -1$ and $\gamma = 4(\mu\omega_T^3)^{1/2}$. Working in units where $\mu = \omega_T = 1$, the box length is $L = 20$ (in each direction), and the grid size is $N^3 = 61^3$. With this, while $\Delta x = L/(N-1) = 0.33$, the time step is $\epsilon = 2\pi(\mu/12)(\Delta x)^2 \approx 0.06$. The left-hand panel gives the full 3D visualization of the number density, whereas the middle and right-hand panels are the number densities as seen in the $y - z$ plane and $x - y$ plane, respectively.

Inclusion of self-interactions. We also investigated the effect of both the spin-dependent and spin-independent self-interactions. The overall effect on the ground state was as expected: when the self-interactions were attractive, the number or spin density compressed, whereas for repulsive self-interactions, the shape of the number or spin density "swelled."

2. Self-trapped BECs with spin-orbit coupling

Our second example concerns the existence of a self-trapped spinor BEC with attractive interaction in free space. Without any confining potentials such as a harmonic trap in the BEC context or gravity in the cosmology context, it is well known that in dimensions 2 and above, the GPE system does not admit bound solitonic states with attractive self-interactions only.[11] However, a novel way to realize such (quasistable) bound states in high dimensions without any trapping potential was presented in Refs. [83,84] for a two-component GPE system, where the stability is provided by means of a SO coupling term. Generalizing the framework to a general spin-s system, the energy is

$$H = \int d^3x \left[\frac{1}{2\mu} \nabla\psi_n^\dagger \cdot \nabla\psi_n - \frac{1}{2\mu^2}(\lambda\rho^2 + \alpha\,(\boldsymbol{\mathcal{S}}\cdot\boldsymbol{\mathcal{S}})) \right.$$
$$\left. - i\,g_{ij}\,\psi_n^\dagger\,[\hat{S}_i]_{nn'}\,\nabla_j\,\psi_{n'} \right]. \tag{45}$$

To simplify matters, here we only consider the case when the SO coupling operator reduces to the helicity operator, i.e., $g_{ij} = g\delta_{ij}$ giving $g_{ij}\hat{S}_i\nabla_j = g\hat{\boldsymbol{S}}\cdot\nabla$. In order to analyze the structure of quasistable bound states (if any), consider field solutions with some characteristic size R and total particle number N. The three different energy terms, corresponding to

the usual pressure, self-interactions, and SO coupling, become

$$H_{\text{kin}} = c_{\text{kin}}\frac{N}{\mu R^2}\,,$$

$$H_{\text{self}} = -\frac{N^2}{\mu^2 R^3}(\lambda c_{\text{si}} + \alpha c_{\text{sd}})\,,$$

$$H_{\text{so}} = -gc_{\text{so}}\frac{N}{R}\,, \tag{46}$$

with the total energy equal to the sum of the three, $H = H_{\text{kin}} + H_{\text{self}} + H_{\text{so}}$, and where the different c's are positive constants. It can be easily seen that for a fixed N, the energy function (as a function of R) admits a local minimum at

$$\mu R = \frac{c_{\text{kin}}}{gc_{\text{so}}} + \frac{1}{gc_{\text{so}}}\left(c_{\text{kin}}^2 - 3gc_{\text{so}}(\lambda c_{\text{si}} + \alpha c_{\text{sd}})N\right)^{1/2}, \tag{47}$$

implying $N < c_{\text{kin}}^2(3gc_{\text{so}}(\lambda c_{\text{si}} + \alpha c_{\text{sd}}))^{-1}$ as the necessary condition for its existence.[12]

In Fig. 2 we show a quasistable state obtained for Hamiltonian (45) (by evolving the field with imaginary time starting from a similar initial condition as the previous example, together with renormalizing the field at every iteration), for a spin-1 system. We note that the obtained state, when evolved in real time, had some very mild time dependence. In order to test the stability of this state, we changed the boundary conditions to both absorptive and reflective (instead of periodic, in which case both mass and spin are of course perfectly conserved). With total energy $\simeq -0.8$ and absorptive boundaries, the object only lost about $10^{-4}\%$ of its total norm within $\sim$33 oscillation cycles (in real time evolution). In Appendix C

---

[11]Although such states can exist in one spatial dimension [79–82].

[12]It must be noted that if self-interactions are absent, the assumption of bound states and hence the scaling argument breaks down. This is because in this case the Hamiltonian commutes with the momentum operator, rendering any possible eigenstate of H to be dispersive and/or nonstationary.
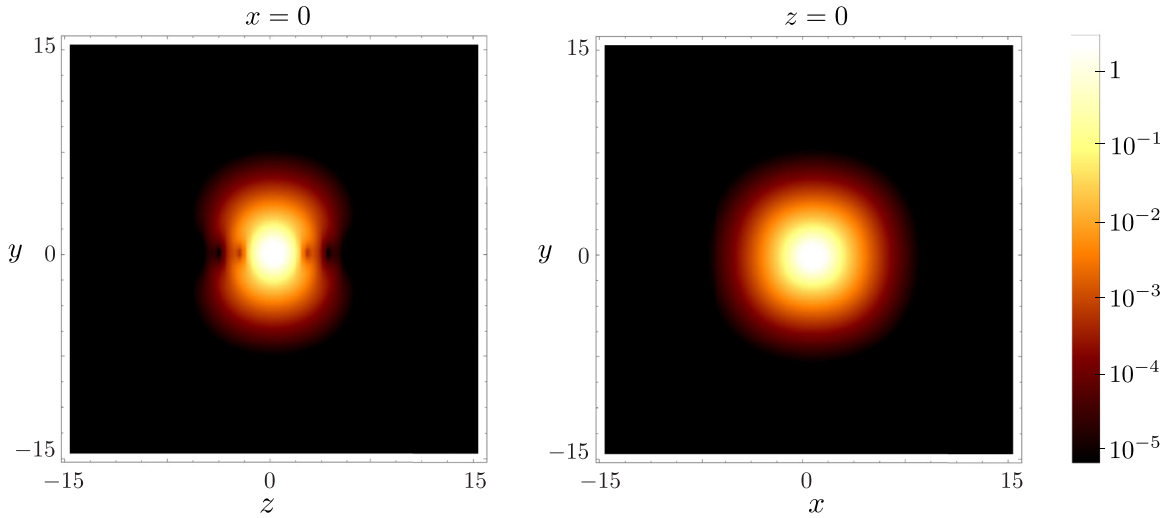
FIG. 2. A stationary state of the Hamiltonian density (46) for a spin-1 system. Working in units where $\mu = 1$, $g_{ij} = 2\delta_{ij}$, $\lambda = 3$, and $\alpha = 0$, the box length is $L = 30$ in each direction and the grid is $N^3 = 81^3$. With this, while $\Delta x = L/(N-1) = 0.375$, the time step is $\epsilon = 2\pi(\mu/12)(\Delta x)^2 \approx 0.074$. The state has a cylindrical symmetry (about the z axis). The left-hand panel shows the number density as seen in the $x-z$ plane (or equivalently $y-z$ plane), whereas the right-hand panel shows the number density in the $x-y$ plane.

we provide mass and spin conservation plots for all three boundary conditions.[13]

B. Cosmological and astrophysical systems

In the contemporary universe, dark matter can be described by a classical, nonrelativistic, bosonic spin-s field [22]. The action in Eq. (1) can be used to explore the dynamics of such dark matter. In this section, we briefly explore the applications and limitations of using Eq. (1) and our corresponding algorithm for exploring dark matter dynamics in an astrophysical and cosmological context. For simplicity, we consider the case where such dark matter only interacts gravitationally with the rest of the standard model, but we will allow for nongravitational self-interactions within the dark sector itself.

Gravitational effects. If the spin-s field determines the dominant energy density in a given region,[14] then the potential $V(\mathbf{x}) \to \Phi(t, \mathbf{x})$ can be thought of as the gravitational potential due to the dark matter density itself, which is also the dominant potential determining the dynamics of the dark matter density. Similarly, the $\bar{\mathbf{B}}(t, \mathbf{x})$ can be interpreted as the gravitomagnetic field generated by the dark matter field itself. Given our assumption of nonrelativistic dark matter, the gravitomagnetic effects are expected to be small. Explicitly, for a spatially localized clump of size R and mass M and with maximal spin $M\hbar/\mu$, the gravitomagnetic term is smaller than the gravitational potential term in Eq. (1) by a factor of $\lambda_c^2/R^2 \ll 1$, where $\lambda_c = \hbar/\mu c$ is the reduced Compton wavelength of the underlying dark matter particle. We caution that additional relativistic corrections beyond the ones included in our action are also present and might be equally or more important; a more careful analysis is warranted (similar to Ref. [85] in the context of scalars). Furthermore, while there is a spin-orbit coupling term due to relativistic corrections in the gravitational system (see, for example, Refs. [86,87]), it is not clear whether the spin-orbit coupling term used in this paper can be directly mapped to that one. If the dark matter field is a subdominant source of energy in a given region, then potential V can be appended by stronger gravitational potentials due to sources in the vicinity—including, for example, a black hole. If also rotating, the $\bar{\mathbf{B}}$ could then be the gravitomagnetic field of such a source. Such gravitomagnetic effects from a relativistic source can be probed by our system. Nevertheless, care is needed to make sure that we self-consistently include relativistic corrections to the action as the dark matter field probes the associated effects.

Including self-interactions. We now turn to nongravitational self-interactions of the dark field. The implications of such interactions in an astrophysical or cosmological setting (in particular for higher bosonic fields) have been explored to an extent in earlier papers by some of us [25,55,71]. We review them briefly here, with an eye towards demonstrating the impact of such interactions using our numerical algorithm. For the scalar case with self-interactions and some associated effects, see, for example Refs. [88–96]. The precise form of pointlike self-interactions in the nonrelativistic limit is dictated by the UV structure of the bosonic theory. At the quartic level in the IR, both density-density and spin-spin interactions

---

[13]It must be noted that in this case of SO coupling, the corresponding self-source term $\mathcal{J}' = i\nabla \times \mathcal{S} = \mathbf{p} \times \mathcal{S}$ may lead to a nonconservation of total spin, especially if the boundary conditions are reflective. In this case, any field packet carrying some spin reflects off from the boundary with a change in the direction of $\mathbf{p}$, resulting in a change in $\mathcal{J}'$.

[14]We assume that such a region is small compared to cosmological scales, so cosmological expansion can be ignored. See Sec. 5 in Ref. [71] by some of us on how it can be incorporated in the algorithm.

are possible. They are in fact present in some of the usual constructions of interacting spin-1 field(s). See, for example, Refs. [25,55], where the quartic interaction term of the vector field A^μ takes the form $\sim (A^\mu A_\mu)^2$, resulting in $\alpha = -\lambda/3$ in the nonrelativistic (IR) limit. Even for the case of a massive spin-2 field there are quartic self-interactions [56–62], and it could very well be that both density-density and spin-spin interactions are present in the IR.[15] These interactions play a significant role in determining the ground state of the system at fixed particle number. In particular, solitons with different spin multiplicities are degenerate in energy for fixed particle number in the absence of self-interactions [22]. However, in the presence of self-interactions the degeneracy gets broken [25,55,71]. The physics of higher spin solitons, including their emergence timescales and related applications (see, for example, Refs. [97–100] for the scalar case and Refs. [101,102] for the spin-1 case), merger dynamics and associated production of gravitational waves (see, for example, Ref. [103] for the scalar case and Ref. [104] for the complex spin-1 case), etc., can be strongly affected by pointlike self-interactions. There can also arise important differences when considering merger rates of solitons, as well as the eventual configurations of merged objects. Such results are essential for related quantitative astrophysical predictions—including the small-scale mass function in higher spin bosonic dark matter [23], the generation of electromagnetic radiation from such merged objects [105], etc.

Numerical examples with gravity and self-interactions Polarized ground states. Using our algorithm (with Euclidean time evolution),[16] we have verified that for a spin-1 field with attractive self-interactions as well as gravity, the zero spin-multiplicity soliton is the ground state. In the repulsive interaction case, the ground state is the $+1$ (or -1) spin-multiplicity soliton. This is consistent with our analytical results in Refs. [25,55,71].

Soliton mergers. To explore the effect of self-interactions on mergers, we carry out three simulations of binary soliton mergers with identical initial conditions. In all three cases, the initial solitons are identical, supported by gravitational interactions alone, and with spin density pointing in the x direction. Their centers are located along a diagonal of the xyz coordinate system. See the top panel of Fig. 3. The time evolution of the spin density in the $x - y$ plane is shown for the three simulations in the bottom two panels of Fig. 3 (time runs downward). The left-most frames include only gravitational interactions. The center frames include gravitational interaction and the spin-independent part of the self-interaction, $\lambda \rho^2$. Lastly, in the right-most frames we show results with all three

---

interactions: gravity, spin-independent interaction $\lambda \rho^2$, and spin-spin interaction $\alpha \boldsymbol{\mathcal{S}} \cdot \boldsymbol{\mathcal{S}}$. We use $\alpha = -\lambda/3$, consistent with the low-energy effective theory of the Abelian (heavy-)Higgs model [25,55]. In all three cases, gravity brings the two solitons together. As the profiles overlap, the self-interaction starts playing an important role. The differences in the mergers are evident in the late time frames. It is likely that the fraction of mass emitted during the merger, the timescale of the merger, as well as the final merged object will differ in the three cases (this will be pursued quantitatively elsewhere). We have checked that, in all three cases, spin and mass are conserved to machine precision, demonstrating that our algorithm and the corresponding code deals with self-interactions appropriately. Corresponding plots are included in Appendix C.

VII. SUMMARY AND DISCUSSION

In this paper we have devised a symplectic algorithm employing the well-known split-Fourier technique to evolve arbitrary spin-s Gross-Pitaevskii systems that are relevant for both AMO systems and astrophysics and cosmology. The multicomponent or spinor Schrödinger field $\boldsymbol{\Psi}$ transforms as a vector, in the $(2s + 1)$-dimensional (irreducible) unitary representation of $SO(3)$. With analytic closed-form expressions for arbitrary spin matrix exponentials, we can simulate arbitrary spin-s nonlinear Schrödinger systems containing many different types of field interactions of general interest. We consider interactions up to quartic order in the field $\boldsymbol{\Psi}$, and to leading order in the nonrelativistic limit. At the quadratic level, these include interactions of the field with external scalar and vector potentials (both of which can be spatially varying in general). For example, in the case of AMO systems, the external potentials include harmonic traps and magnetic fields, while in the case of cosmology they include external gravitational potential generated by some source. At the quartic level, we include several interactions, both long and short ranged. For the long-range interactions, we can have the dipolar ($\sim 1/r^3$) self-generated potential in the case of spinor AMO systems, and the Newtonian gravitational ($\sim 1/r$) self-generated potential in the case of ultralight dark matter in cosmology. For short-range (pointlike) interactions, we include both spin-independent and spin-dependent interactions. The former is proportional to the square of the number density, while the latter can be further subdivided into two types: spin-spin interaction being proportional to the norm of the spin density squared, and spin-singlet interaction involving two-particle spin-singlet in and out states. Such interactions are of interest in both AMO systems and integer-spin self-interacting dark matter cosmology. Last, we also include the well-known spin-orbit coupling term relevant for many AMO systems targeted towards studying spinor BECs. We discussed possible applications of our work in a variety of different contexts, both in the study of spinor BECs in AMO physics and dark matter cosmology. For demonstration purposes, we present some simulation results on both of these fronts. For the AMO case, we present ground states for two different scenarios. In the first scenario, the spinor ultracold atomic gas is subject to a synthetic "hedgehog" magnetic field along with a radially symmetric harmonic trap. This leads to the trapping of the field onto a spherical shell along with the emergence of

---

[15]The precise value of the four-point coupling constant λ is dictated by the UV scales. For the spin-1 case with a Higgs mechanism, $\lambda \sim g^2 \mu^2 / M_h^2$, where g and M_h are the gauge coupling and Higgs mass, respectively [25,55]. For the spin-2 bigravity case, $\lambda \sim \mu^2 / m_{\rm pl}^2$ apart from some overall constants [22,63].

[16]In using Euclidean time evolution to find the ground state, we constantly renormalize the field at each time step. In the case where nonlinearities are present, the value by which one renormalizes matters. For example, to construct a soliton with total particle number N, we renormalize the field by $\sqrt{N}$ at every iteration.
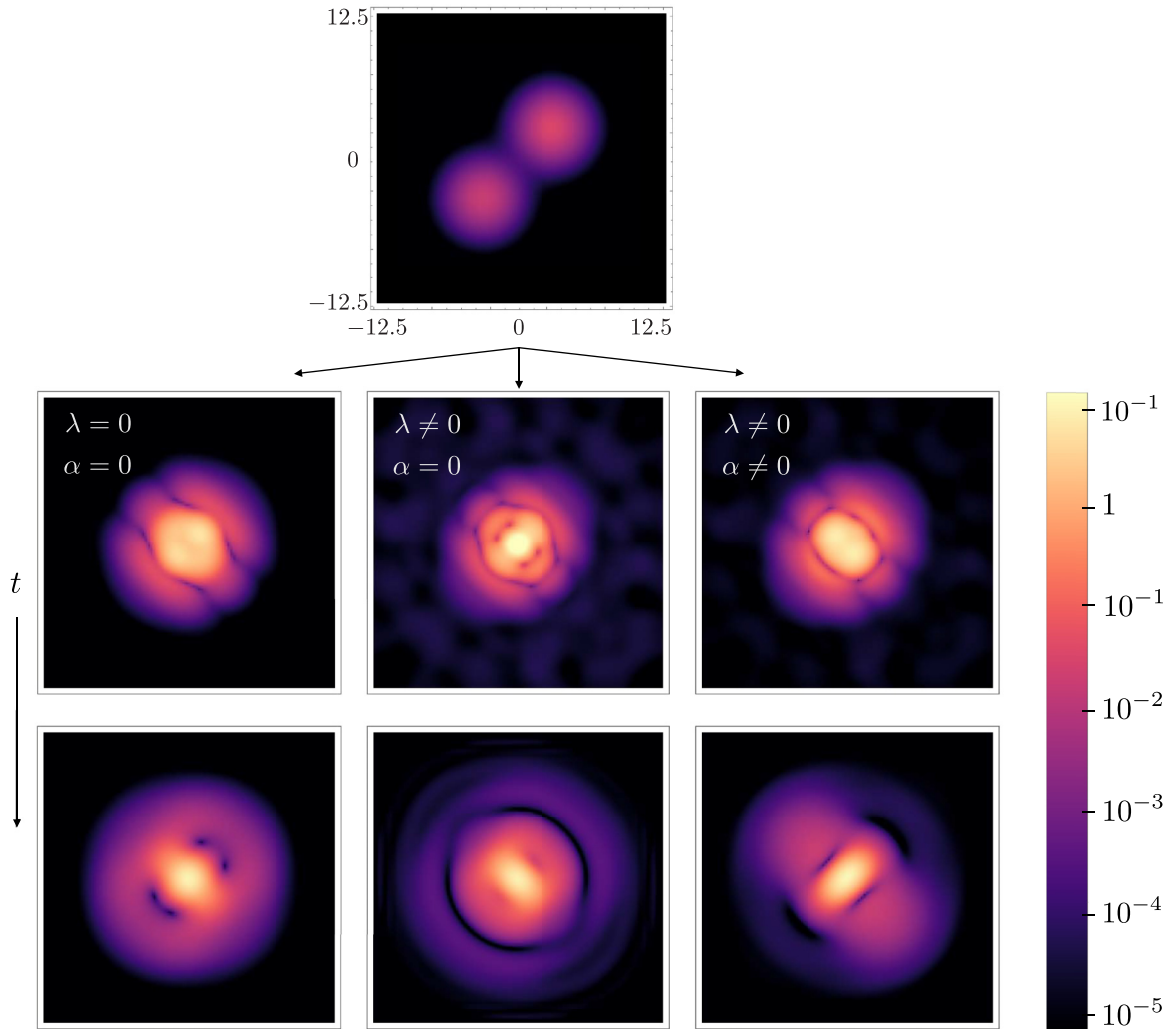
FIG. 3. Spin density at different instants in the collision of two spin-1 solitons, as seen in the $z = 0$ plane. Working in units where $\mu = 1$ and $G = 1/8\pi$, the box length in each direction is $L = 25$ and the grid size is $N^3 = 101^3$. Spatial discretization is $\Delta x = L/(N-1) = 0.25$, while the time step is $\epsilon = 2\pi(\mu/12)(\Delta x)^2 \approx 0.03$. At the start (top figure), two solitons, each of total "mass" 60, were only gravitationally bound, stationary, and diagonally opposite in the $x - y - z$ space. To capture the effects of gravity, spin-independent, and spin-dependent interactions, we performed three simulations. In the left-hand panel, gravitational interactions were included, and pointlike interactions were not. The center panel shows the same scenario but with the addition of spin-independent (attractive) interaction $\propto \lambda\rho^2$ (with $\lambda = 0.03$). Finally, the right-hand panel shows the case when the spin-dependent interaction $\propto \alpha\, \boldsymbol{\mathcal{S}} \cdot \boldsymbol{\mathcal{S}}$ was also included (with $\alpha = -0.01$). The impact of the spin-independent and spin-dependent interactions are accurately captured by our numerical evolution. The two times at which the snapshots (middle and lower panels) are shown are $t \approx 39.5$ and $t \approx 45.2$, respectively. For comparison, note that the gravitational free fall timescale $t_{\rm dyn} \equiv (r^3/GM)^{1/2} \approx 22.3$, where r is the initial separation between the solitons.

Dirac strings due to an effective "magnetic monopole" field (where the spin or hyperfine quantum number of the atoms acts as the charge). In the second scenario, the spinor gas has attractive quartic self-interactions and is only subject to a spin-orbit coupling. Such a setup leads to the creation of quasistable self-bound solitonic states owing to the balancing of gradient pressure with the attractive self-interactions and spin-orbit coupling induced attraction together. For the case of cosmology, we present examples of binary mergers of spin-1 solitons, with a focus on the role played by the different interactions: long-range gravitational self-interactions,

and short-range spin-independent and spin-dependent self-interactions. We see features in the three collision cases which are reflective of the distinct nature of each of the interactions. The split-step Fourier method (also known as the partitioned Runge-Kutta method) discussed in this paper is $O(\epsilon^2)$ accurate, where ϵ is the discrete time step.[17] With the full

---

[17]See Sec. 4.3 of Ref. [101]. While the error at each step is of $O(\epsilon^3)$, the accumulated error grows and the full evolution of the field is only $O(\epsilon^2)$ accurate.

Hamiltonian broken into drift and kick Hamiltonian pieces [cf. Eqs. (7)], the accuracy of the integrator can be extended by applying the kick and drift operations in succession, with appropriately chosen coefficients in the respective exponents [106]. We believe that the method we developed here can be used in a wide range of fields.

APPENDIX A: CONVENTIONAL SPIN MATRICES FOR BOSONIC FIELD THEORIES

From a field-theoretic point of view, and specializing towards massive vector (spin-1) and tensor (spin-2) cases, the field components are usually expressed in a Cartesian basis. The spin angular momentum in the nonrelativistic limit is [22]

$$\mathcal{S}_k = s\,i\,\varepsilon_{ijk}[\mathbf{\Psi}\,\mathbf{\Psi}^\dagger]_{ij}\,. \tag{A1}$$

Here ε is the Levi-Cività symbol, and the quantity $[\mathbf{\Psi}\,\mathbf{\Psi}^\dagger]_{ij} = \psi_i\psi_j^*$ for the vector, while $[\mathbf{\Psi}\,\mathbf{\Psi}^\dagger]_{ij} = \psi_{ik}\psi_{jk}^*$ for the tensor case. From this, we can obtain the spin matrices by decomposing the field $\mathbf{\Psi}$ in the spin basis using the polarization vectors and tensors [22]:

$$\mathbf{\Psi} = \sum_{m=-s}^{s} \psi_m\,\boldsymbol{\epsilon}_{s,\hat{n}}^{(m)}\,. \tag{A2}$$

The set $\{\boldsymbol{\epsilon}_{s,\hat{n}}^m\}$ is orthogonal and complete. That is, we have

$$\mathrm{Tr}\big[\boldsymbol{\epsilon}_{s,\hat{n}}^{(m')\,\dagger}\,\boldsymbol{\epsilon}_{s,\hat{n}}^{(m)}\big] = \delta_{m'm}\,,$$
$$\sum_m \big[\boldsymbol{\epsilon}_{s,\hat{n}}^{(m)}\,\boldsymbol{\epsilon}_{s,\hat{n}}^{(m)\dagger}\big]_{ij} = \frac{2s+1}{3}\delta_{ij}\,. \tag{A3}$$

Using ansatz (A2) in Eq. (A1), and identifying $\mathcal{S}_k \equiv \psi_{m'}^*[\hat{S}_k']_{m'm}\psi_m$, we get the following form for the spin matrices:

$$[\hat{S}_k']_{mm'} = s\,i\,\varepsilon_{ijk}\big[\boldsymbol{\epsilon}_{s,\hat{n}}^{(m')}\,\boldsymbol{\epsilon}_{s,\hat{n}}^{(m)\,\dagger}\big]_{ij}\,. \tag{A4}$$

Working with the explicit forms of the polarization tensors $\boldsymbol{\epsilon}$ for the spin-1 and spin-2 cases, respectively, it can be seen that the spin matrices (A5) indeed have the desired Lie algebra of the $SO(3)$ group, and the total spin squared matrix is equal to $s(s+1)$ times the identity. That is,

$$[\hat{S}_x', \hat{S}_y'] = i\hat{S}_z' \qquad \text{with all cyclic permutations,}$$
$$\hat{\mathbf{S}}' \cdot \hat{\mathbf{S}}' = s(s+1)\mathbb{I}_{N\times N}, \qquad N = 2s+1\,. \tag{A5}$$

In the next two sections we give the explicit forms for the spin-1 and spin-2 cases.

1. Spin-1 case

In our working (z) basis, the polarization vectors $\boldsymbol{\epsilon}$ take the following conventional form [22]:

$$\boldsymbol{\epsilon}_{1,\hat{z}}^{(\pm1)} = \frac{1}{\sqrt{2}}\begin{pmatrix}1\\ \pm i\\ 0\end{pmatrix}, \qquad \boldsymbol{\epsilon}_{1,\hat{z}}^{(0)} = \begin{pmatrix}0\\ 0\\ 1\end{pmatrix}. \tag{A6}$$

Using these in Eq. (A5), we get the following explicit forms for the spin matrices:

$$\hat{S}_x' = \frac{1}{\sqrt{2}}\begin{pmatrix}0 & -1 & 0\\ -1 & 0 & 1\\ 0 & 1 & 0\end{pmatrix}, \; \hat{S}_y' = \frac{i}{\sqrt{2}}\begin{pmatrix}0 & 1 & 0\\ -1 & 0 & -1\\ 0 & 1 & 0\end{pmatrix},$$
$$\hat{S}_z' = \begin{pmatrix}1 & 0 & 0\\ 0 & 0 & 0\\ 0 & 0 & -1\end{pmatrix}. \tag{A7}$$

It can be seen that with the above, we do have relations (A5) atisfied.

2. Spin-2 case

For the tensor case, the polarization tensors can be obtained using the spin-1 polarization vectors as

$$\boldsymbol{\epsilon}_{2,\hat{z}}^{(\pm2)} = \frac{1}{\sqrt{2}}\big(\epsilon_{1,\hat{z}}^{(\pm1)} \otimes \epsilon_{1,\hat{z}}^{(\pm1)}\big),$$
$$\boldsymbol{\epsilon}_{2,\hat{z}}^{(0)} = \frac{1}{\sqrt{6}}\big(2\epsilon_{1,\hat{z}}^{(0)} \otimes \epsilon_{1,\hat{z}}^{(0)} - \epsilon_{1,\hat{z}}^{(1)} \otimes \epsilon_{1,\hat{z}}^{(-1)} - \epsilon_{1,\hat{z}}^{(-1)} \otimes \epsilon_{1,\hat{z}}^{(1)}\big),$$
$$\boldsymbol{\epsilon}_{2,\hat{z}}^{(\pm1)} = \frac{1}{\sqrt{2}}\big(\epsilon_{1,\hat{z}}^{(0)} \otimes \epsilon_{1,\hat{z}}^{(\pm1)} + \epsilon_{1,\hat{z}}^{(\pm1)} \otimes \epsilon_{1,\hat{z}}^{(0)}\big), \tag{A8}$$

and take the following form [22]:

$$\boldsymbol{\epsilon}_{2,\hat{z}}^{(\pm2)} = \frac{1}{2}\begin{pmatrix}1 & \pm i & 0\\ \pm i & -1 & 0\\ 0 & 0 & 0\end{pmatrix}, \boldsymbol{\epsilon}_{2,\hat{z}}^{(\pm1)} = \frac{1}{2}\begin{pmatrix}0 & 0 & 1\\ 0 & 0 & \pm i\\ 1 & \pm i & 0\end{pmatrix}, \boldsymbol{\epsilon}_{2,\hat{z}}^{(0)} = \frac{1}{\sqrt{6}}\begin{pmatrix}-1 & 0 & 0\\ 0 & -1 & 0\\ 0 & 0 & 2\end{pmatrix}. \tag{A9}$$

With these, the spin matrices evaluate to [cf. Eq. (A5)]

$$\hat{S}_x' = \begin{pmatrix}0 & -1 & 0 & 0 & 0\\ -1 & 0 & -\sqrt{\frac{3}{2}} & 0 & 0\\ 0 & -\sqrt{\frac{3}{2}} & 0 & \sqrt{\frac{3}{2}} & 0\\ 0 & 0 & \sqrt{\frac{3}{2}} & 0 & 1\\ 0 & 0 & 0 & 1 & 0\end{pmatrix}, \hat{S}_y' = i\begin{pmatrix}0 & 1 & 0 & 0 & 0\\ -1 & 0 & \sqrt{\frac{3}{2}} & 0 & 0\\ 0 & -\sqrt{\frac{3}{2}} & 0 & -\sqrt{\frac{3}{2}} & 0\\ 0 & 0 & \sqrt{\frac{3}{2}} & 0 & -1\\ 0 & 0 & 0 & 1 & 0\end{pmatrix},$$

$$\hat{S}'_z = \begin{pmatrix} 2 & 0 & 0 & 0 & 0 \\ 0 & 1 & 0 & 0 & 0 \\ 0 & 0 & 0 & 0 & 0 \\ 0 & 0 & 0 & -1 & 0 \\ 0 & 0 & 0 & 0 & -2 \end{pmatrix}. \tag{A10}$$

Once again it can be easily seen that relations (A5) are satisfied.

APPENDIX B: EXPLICIT MATRIX EXPONENTIALS FOR SPIN-1, SPIN-2, AND SPIN-3 CASES

1. Spin-1 case

For spin-1 systems, the exponential matrix has the following analytical solution:[18]

$$e^{-i\beta\,\hat{\boldsymbol{n}}\cdot\hat{\boldsymbol{S}}} = \mathbb{I}_{3\times3} - i(\hat{\boldsymbol{n}}\cdot\hat{\boldsymbol{S}})\sin\beta + (\hat{\boldsymbol{n}}\cdot\hat{\boldsymbol{S}})^2(-1+\cos\beta), \tag{B1}$$

where

$$\hat{\boldsymbol{n}}\cdot\hat{\boldsymbol{S}} = \begin{pmatrix} n_z & \frac{n_x}{\sqrt{2}} - \frac{in_y}{\sqrt{2}} & 0 \\ \frac{n_x}{\sqrt{2}} + \frac{in_y}{\sqrt{2}} & 0 & \frac{n_x}{\sqrt{2}} - \frac{in_y}{\sqrt{2}} \\ 0 & \frac{n_x}{\sqrt{2}} + \frac{in_y}{\sqrt{2}} & -n_z \end{pmatrix}. \tag{B2}$$

2. Spin-2 case

For spin-2 systems, we have the following closed-form expression:

$$e^{-i\beta\,\hat{\boldsymbol{n}}\cdot\hat{\boldsymbol{S}}} = \mathbb{I}_{5\times5} + i(\hat{\boldsymbol{n}}\cdot\hat{\boldsymbol{S}})\left(-\frac{4}{3}\sin\beta + \frac{1}{6}\sin2\beta\right) + (\hat{\boldsymbol{n}}\cdot\hat{\boldsymbol{S}})^2\left(-\frac{5}{4} + \frac{4}{3}\cos\beta - \frac{1}{12}\cos2\beta\right)$$

$$+ i(\hat{\boldsymbol{n}}\cdot\hat{\boldsymbol{S}})^3\left(\frac{1}{3}\sin\beta - \frac{1}{6}\sin2\beta\right) + (\hat{\boldsymbol{n}}\cdot\hat{\boldsymbol{S}})^4\left(\frac{1}{4} - \frac{1}{3}\cos\beta + \frac{1}{12}\cos2\beta\right),$$

where

$$\hat{\boldsymbol{n}}\cdot\hat{\boldsymbol{S}} = \begin{pmatrix} 2n_z & n_x - in_y & 0 & 0 & 0 \\ n_x + in_y & n_z & \sqrt{\frac{3}{2}}n_x - i\sqrt{\frac{3}{2}}n_y & 0 & 0 \\ 0 & \sqrt{\frac{3}{2}}n_x + i\sqrt{\frac{3}{2}}n_y & 0 & \sqrt{\frac{3}{2}}n_x - i\sqrt{\frac{3}{2}}n_y & 0 \\ 0 & 0 & \sqrt{\frac{3}{2}}n_x + i\sqrt{\frac{3}{2}}n_y & -n_z & n_x - in_y \\ 0 & 0 & 0 & n_x + in_y & -2n_z \end{pmatrix}. \tag{B3}$$

3. Spin-3 case

For the spin-3 case, we get the following closed-form expression:

$$e^{-i\beta\,\hat{\boldsymbol{n}}\cdot\hat{\boldsymbol{S}}} = \mathbb{I}_{7\times7} + i(\hat{\boldsymbol{n}}\cdot\hat{\boldsymbol{S}})\left(-\frac{3}{2}\sin\beta + \frac{3}{10}\sin2\beta - \frac{1}{30}\sin3\beta\right) + (\hat{\boldsymbol{n}}\cdot\hat{\boldsymbol{S}})^2\left(-\frac{49}{36} + \frac{3}{2}\cos\beta - \frac{3}{20}\cos2\beta + \frac{1}{90}\cos3\beta\right)$$

$$+ i(\hat{\boldsymbol{n}}\cdot\hat{\boldsymbol{S}})^3\left(\frac{13}{24}\sin\beta - \frac{1}{3}\sin2\beta + \frac{1}{24}\sin3\beta\right) + (\hat{\boldsymbol{n}}\cdot\hat{\boldsymbol{S}})^4\left(\frac{7}{18} - \frac{13}{24}\cos\beta + \frac{1}{6}\cos2\beta - \frac{1}{72}\cos3\beta\right)$$

$$+ i(\hat{\boldsymbol{n}}\cdot\hat{\boldsymbol{S}})^5\left(-\frac{1}{24}\sin\beta + \frac{1}{30}\sin2\beta - \frac{1}{120}\sin3\beta\right) + (\hat{\boldsymbol{n}}\cdot\hat{\boldsymbol{S}})^6\left(-\frac{1}{36} + \frac{1}{24}\cos\beta - \frac{1}{60}\cos2\beta + \frac{1}{360}\cos3\beta\right), \tag{B4}$$

---

[18]For the spin-1/2 case where $\hat{\boldsymbol{S}} = \hat{\boldsymbol{\sigma}}/2$, the matrix exponential is the same as in Eq. (B3) with the replacements $\mathbb{I}_{3\times3} \to \mathbb{I}_{2\times2}$, $\hat{\boldsymbol{n}}\cdot\hat{\boldsymbol{S}} \to 2\,\hat{\boldsymbol{n}}\cdot\hat{\boldsymbol{S}}$, and $\beta \to \beta/2$ in the right-hand side of Eq. (B3).
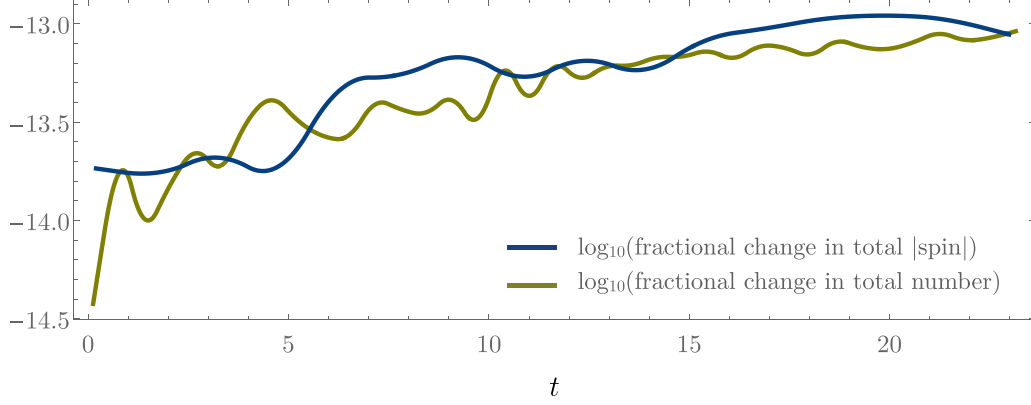
FIG. 4. Plot showing conservation of total particle number and spin magnitude (up to machine precision), for the state shown in Fig. 1. In general this demonstrates satisfactory performance of our algorithm for handling a Zeeman term with arbitrary spatially dependent magnetic field (with any overall time dependence). Note that the vertical is a logarithm of the fractional change in conserved quantities and that mass and spin are conserved to one part in 10^{13}.

where

$$
\hat{\boldsymbol{n}} \cdot \hat{\boldsymbol{S}} = \begin{pmatrix} 3n_z & \sqrt{\frac{3}{2}}n_x - i\sqrt{\frac{3}{2}}n_y & 0 & 0 & 0 & 0 & 0 \\ \sqrt{\frac{3}{2}}n_x + i\sqrt{\frac{3}{2}}n_y & 2n_z & \sqrt{\frac{5}{2}}n_x - i\sqrt{\frac{5}{2}}n_y & 0 & 0 & 0 & 0 \\ 0 & \sqrt{\frac{5}{2}}n_x + i\sqrt{\frac{5}{2}}n_y & n_z & \sqrt{3}n_x - i\sqrt{3}n_y & 0 & 0 & 0 \\ 0 & 0 & \sqrt{3}n_x + i\sqrt{3}n_y & 0 & \sqrt{3}n_x - i\sqrt{3}n_y & 0 & 0 \\ 0 & 0 & 0 & \sqrt{3}n_x + i\sqrt{3}n_y & -n_z & \sqrt{\frac{5}{2}}n_x - i\sqrt{\frac{5}{2}}n_y & 0 \\ 0 & 0 & 0 & 0 & \sqrt{\frac{5}{2}}n_x + i\sqrt{\frac{5}{2}}n_y & -2n_z & \sqrt{\frac{3}{2}}n_x - i\sqrt{\frac{3}{2}}n_y \\ 0 & 0 & 0 & 0 & 0 & \sqrt{\frac{3}{2}}n_x + i\sqrt{\frac{3}{2}}n_y & -3n_z \end{pmatrix}. \quad (B5)
$$

In general with relations (34) and (35) for the coefficients appearing in the exponential of the spin matrices (33), and the expression (8) for the spin matrices, we can easily get analytical forms for $e^{-i\beta\,\hat{\boldsymbol{n}}\cdot\hat{\boldsymbol{S}}}$ for any arbitrary integer spin system.

APPENDIX C: PERFORMANCE PLOTS

In this Appendix, in order to demonstrate the fidelity of our scheme, we present both mass and spin conservation for the three cases presented in the main text. Figure 4 presents the fractional change in the total mass and norm of the total spin as a function of time, when the obtained stationary state, as shown in Fig. 1 for the effective magnetic monopole case, is evolved through real time. Figure 5 shows the same quantities for the quasistable state obtained for our spin-orbit coupling case (see Fig. 2), when evolved through real time. Finally, in Fig. 6 we show the fractional change in total mass and norm of the total spin, for the case
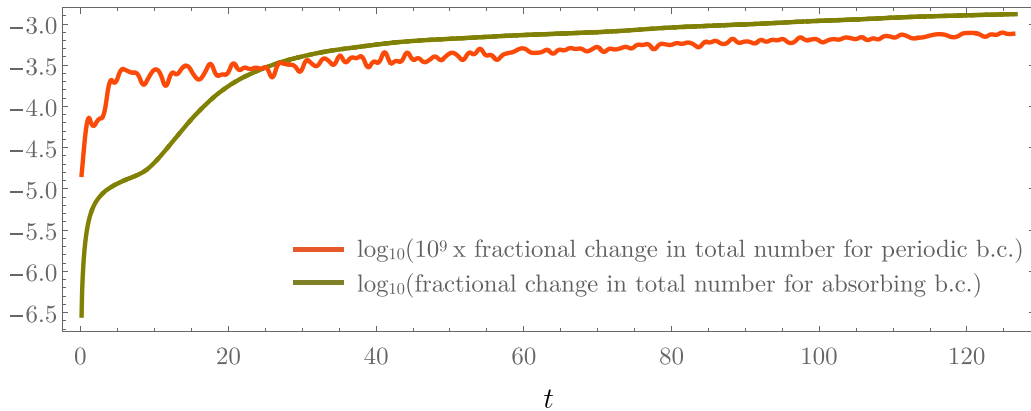

FIG. 5. Plot showing conservation of total particle number for the quasistable state shown in Fig. 2. As mentioned in the main text, the state has a very mild time dependence due to which it tends to dissipate energy towards the boundary. This effect is captured by imposing absorbing boundary conditions leading to nonconservation of total particle number. For periodic boundary conditions, the total number is once again preserved up to machine precision. As noted in the legend, the vertical axis is $\log(\cdot)$ of respective quantities.
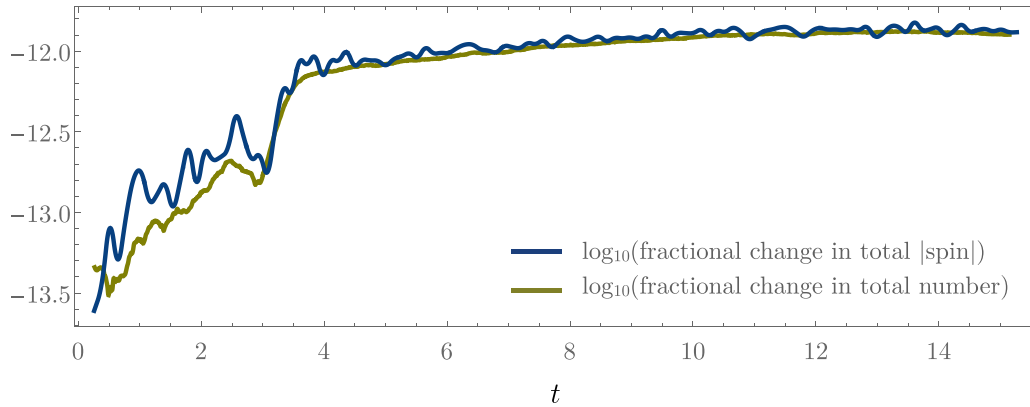
FIG. 6. Same plot as Fig. 4, for the two spin-1 soliton collision scenario presented in Fig. 3, including gravitational self-interactions, and both the density-density and spin-spin short-range self-interactions (corresponding to the right-most panel of Fig. 3). As seen in the plots, the preservation of mass and spin in this case is at the order of 10^{-12}.

of a two-soliton collision shown in Fig. 3 (with all interactions turned on), while in Fig. 7 we show the reversibility feature of the algorithm (for the same collision scenario). Similarly as in Ref. [101], we have defined the reversibility factor, $\gamma(t)$, as

$$\gamma(t) \equiv \left(\frac{1}{N} \int \mathrm{d}^3 x \, |\boldsymbol{\Psi}_+(\boldsymbol{x}, t) - \boldsymbol{\Psi}_-(\boldsymbol{x}, t)|^2 \right)^{1/2}. \tag{C1}$$

Here N is the total rescaled mass (which is already conserved up to machine precision as shown above); the subscript "+" denotes the forward evolved field starting from some initial condition $\boldsymbol{\Psi}(\boldsymbol{x}, t_i)$ up to a final configuration $\boldsymbol{\Psi}(\boldsymbol{x}, t_f)$, while the subscript "−" denotes the reverse evolved field, starting from the initial condition $\boldsymbol{\Psi}(\boldsymbol{x}, t_f)$ and time reversed ($\epsilon \to -\epsilon$ in the simulation). As is evident, this factor gives a direct measure of the separation between the forward and backward field trajectories in state space.

All of these curves reflects the fidelity of the symplectic and reversible nature of our algorithm, containing many different types of field self-interactions that are relevant in both AMO systems and light-dark matter cosmology.
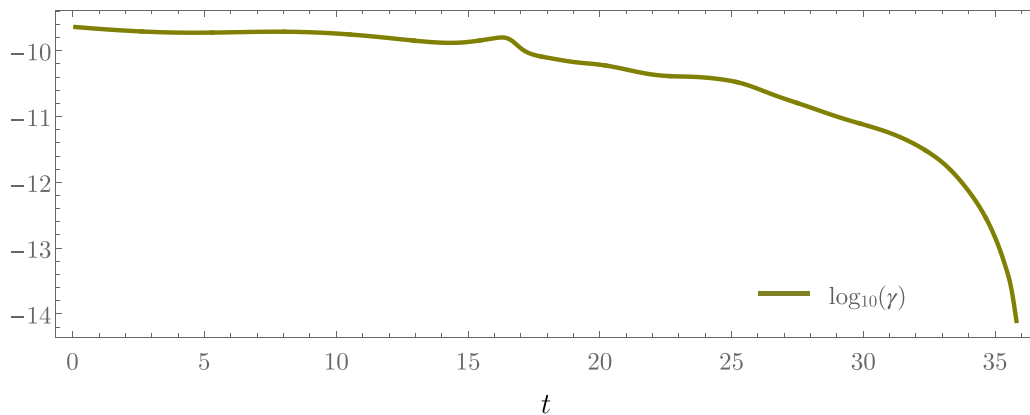

FIG. 7. A (logarithmic) plot of the reversibility factor $\gamma(t)$, for the two spin-1 soliton collision scenario for all interactions, where γ is defined in Eq. (C1).

[1] F. Dalfovo, S. Giorgini, L. P. Pitaevskii, and S. Stringari, Theory of Bose-Einstein condensation in trapped gases, Rev. Mod. Phys. **71**, 463 (1999).

[2] G. P. Agrawal, Nonlinear fiber optics, in *Nonlinear Science at the Dawn of the 21st Century*, edited by P. L. Christiansen, M. P. Sørensen, and A. C. Scott (Springer, Berlin, 2000), pp. 195–211.

[3] C. Menyuk, Nonlinear pulse propagation in birefringent optical fibers, IEEE J. Quantum Electron. **23**, 174 (1987).

[4] D. N. Christodoulides and R. Joseph, Vector solitons in birefringent nonlinear dispersive media, Opt. Lett. **13**, 53 (1988).

[5] D. Rand, I. Glesk, C.-S. Brès, D. A. Nolan, X. Chen, J. Koh, J. W. Fleischer, K. Steiglitz, and P. R. Prucnal, Observation of

temporal vector soliton propagation and collision in birefringent fiber, Phys. Rev. Lett. **98**, 053902 (2007).

[6] Z.-Y. Sun, Y.-T. Gao, X. Yu, W.-J. Liu, and Y. Liu, Bound vector solitons and soliton complexes for the coupled nonlinear Schrödinger equations, Phys. Rev. E **80**, 066608 (2009).

[7] F. Baronio, A. Degasperis, M. Conforti, and S. Wabnitz, Solutions of the vector nonlinear Schrödinger equations: Evidence for deterministic rogue waves, Phys. Rev. Lett. **109**, 044102 (2012).

[8] S. V. Manakov, On the theory of two-dimensional stationary self-focusing of electromagnetic waves, Zh. Eksp. Teor. Fiz. **65**, 505 (1973).

[9] D. J. Benney and A. C. Newell, The propagation of nonlinear wave envelopes, J. Math. Phys. **46**, 133 (1967).

[10] G. J. Roskes, Some nonlinear multiphase interactions, Stud. Appl. Math. **55**, 231 (1976).

[11] K. Dysthe, H. E. Krogstad, and P. Müller, Oceanic rogue waves, Annu. Rev. Fluid Mech. **40**, 287 (2008).

[12] M. S. Turner, Coherent scalar field oscillations in an expanding universe, Phys. Rev. D **28**, 1243 (1983).

[13] W. H. Press, B. S. Ryden, and D. N. Spergel, Single mechanism for generating large scale structure and providing dark missing matter, Phys. Rev. Lett. **64**, 1084 (1990).

[14] S.-J. Sin, Late time cosmological phase transition and galactic halo as Bose liquid, Phys. Rev. D **50**, 3650 (1994).

[15] J. Goodman, Repulsive dark matter, New Astron. **5**, 103 (2000).

[16] F. S. Guzman and L. A. Urena-Lopez, Newtonian collapse of scalar field dark matter, Phys. Rev. D **68**, 024023 (2003).

[17] L. Amendola and R. Barbieri, Dark matter from an ultra-light pseudo-Goldsone-boson, Phys. Lett. B **642**, 192 (2006).

[18] E. Calabrese and D. N. Spergel, Ultra-light dark matter in ultra-faint dwarf galaxies, Mon. Not. R. Astron. Soc. **460**, 4397 (2016).

[19] J. C. Niemeyer, Small-scale structure of fuzzy and axion-like dark matter, Prog. Part. Nucl. Phys. **113**, 103787 (2020).

[20] E. G. M. Ferreira, Ultra-light dark matter, Astron. Astrophys. Rev. **29**, 7 (2021).

[21] P. Adshead and K. D. Lozanov, Self-gravitating vector dark matter, Phys. Rev. D **103**, 103501 (2021).

[22] M. Jain and M. A. Amin, Polarized solitons in higher-spin wave dark matter, Phys. Rev. D **105**, 056019 (2022).

[23] M. A. Amin, M. Jain, R. Karur, and P. Mocz, Small-scale structure in vector dark matter, J. Cosmol. Astropart. Phys. 08 (2022) 014.

[24] M. Gorghetto, E. Hardy, J. March-Russell, N. Song, and S. M. West, Dark photon stars: Formation and role as dark matter substructure, J. Cosmol. Astropart. Phys. 08 (2022) 018.

[25] M. Jain, Soliton stars in Yang-Mills-Higgs theories, Phys. Rev. D **106**, 085011 (2022).

[26] D. M. Stamper-Kurn, M. R. Andrews, A. P. Chikkatur, S. Inouye, H.-J. Miesner, J. Stenger, and W. Ketterle, Optical confinement of a Bose-Einstein condensate, Phys. Rev. Lett. **80**, 2027 (1998).

[27] C. K. Law, H. Pu, and N. P. Bigelow, Quantum spins mixing in spinor Bose-Einstein condensates, Phys. Rev. Lett. **81**, 5257 (1998).

[28] D. M. Stamper-Kurn and M. Ueda, Spinor Bose gases: Symmetries, magnetism, and quantum dynamics, Rev. Mod. Phys. **85**, 1191 (2013).

[29] C. J. Myatt, E. A. Burt, R. W. Ghrist, E. A. Cornell, and C. E. Wieman, Production of two overlapping Bose-Einstein condensates by sympathetic cooling, Phys. Rev. Lett. **78**, 586 (1997).

[30] Y. Lin, K. Jiménez-García, and I. Spielman, Spin-orbit-coupled Bose-Einstein condensates, Nature (London) **471**, 83 (2011).

[31] J. Stenger, S. Inouye, D. Stamper-Kurn, H. Miesner, A.P.Chikkatur, and W. Ketterle, Spin domains in ground-state Bose-Einstein condensates, Nature (London) **396**, 345 (1998).

[32] M. D. Barrett, J. A. Sauer, and M. S. Chapman, All-optical formation of an atomic Bose-Einstein condensate, Phys. Rev. Lett. **87**, 010404 (2001).

[33] C. Samuelis, E. Tiesinga, T. Laue, M. Elbs, H. Knöckel, and E. Tiemann, Cold atomic collisions studied by molecular spectroscopy, Phys. Rev. A **63**, 012710 (2000).

[34] M.-S. Chang, C. D. Hamley, M. D. Barrett, J. A. Sauer, K. M. Fortier, W. Zhang, L. You, and M. S. Chapman, Observation of spinor dynamics in optically trapped ^{87}Rb Bose-Einstein condensates, Phys. Rev. Lett. **92**, 140403 (2004).

[35] H. Schmaljohann, M. Erhard, J. Kronjäger, M. Kottke, S. van Staa, L. Cacciapuoti, J. J. Arlt, K. Bongs, and K. Sengstock, Dynamics of $f = 2$ spinor Bose-Einstein condensates, Phys. Rev. Lett. **92**, 040402 (2004).

[36] A. Widera, F. Gerbier, S. Fölling, T. Gericke, O. Mandel, and I. Bloch, Precision measurement of spin-dependent interaction strengths for spin-1 and spin-2 ^{87}Rb atoms, New J. Phys. **8**, 152 (2006).

[37] K. C. Wright, L. S. Leslie, and N. P. Bigelow, Optical control of the internal and external angular momentum of a Bose-Einstein condensate, Phys. Rev. A **77**, 041601(R) (2008).

[38] B. Pasquiou, G. Bismut, Q. Beaufils, A. Crubellier, E. Maréchal, P. Pedri, L. Vernac, O. Gorceix, and B. Laburthe-Tolra, Control of dipolar relaxation in external fields, Phys. Rev. A **81**, 042716 (2010).

[39] B. Pasquiou, E. Maréchal, G. Bismut, P. Pedri, L. Vernac, O. Gorceix, and B. Laburthe-Tolra, Spontaneous demagnetization of a dipolar spinor Bose gas in an ultralow magnetic field, Phys. Rev. Lett. **106**, 255303 (2011).

[40] S. Kang, S. W. Seo, H. Takeuchi, and Y. Shin, Observation of wall-vortex composite defects in a spinor Bose-Einstein condensate, Phys. Rev. Lett. **122**, 095301 (2019).

[41] M. W. Ray, E. Ruokokoski, K. Tiurev, M. Möttönen, and D. S. Hall, Observation of isolated monopoles in a quantum field, Science **348**, 544 (2015).

[42] Y. K. Kato, R. C. Myers, A. C. Gossard, and D. D. Awschalom, Observation of the spin Hall effect in semiconductors, Science **306**, 1910 (2004).

[43] M. König, S. Wiedmann, C. Brüne, A. Roth, H. Buhmann, L. W. Molenkamp, X.-L. Qi, and S.-C. Zhang, Quantum spin Hall insulator state in HgTe quantum wells, Science **318**, 766 (2007).

[44] C. L. Kane and E. J. Mele, Z_2 topological order and the quantum spin Hall effect, Phys. Rev. Lett. **95**, 146802 (2005).

[45] B. A. Bernevig, T. L. Hughes, and S.-C. Zhang, Quantum spin Hall effect and topological phase transition in HgTe quantum wells, Science **314**, 1757 (2006).

[46] D. Hsieh, D. Qian, L. Wray, Y. Xia, Y. Hor, R. Cava, and M. Hasan, A topological Dirac insulator in a quantum spin Hall phase, Nature (London) **452**, 970 (2008).

[47] I. Bloch, T. W. Hänsch, and T. Esslinger, Atom laser with a cw output coupler, Phys. Rev. Lett. **82**, 3008 (1999).

[48] V. Bolpasi, N. K. Efremidis, M. J. Morrissey, P. Condylis, D. Sahagun, M. Baker, and W. von Klitzing, An ultra-bright atom laser, New J. Phys. **16**, 033036 (2014).

[49] Y. Kawaguchi and M. Ueda, Spinor Bose-Einstein condensates, Phys. Rep. **520**, 253 (2012).

[50] M. Ueda, Topological aspects in spinor Bose-Einstein condensates, Rep. Prog. Phys. **77**, 122401 (2014).

[51] W. Bao and Y. Cai, Mathematical models and numerical methods for spinor Bose-Einstein condensates, Commun. Comput. Phys. **24**, 899 (2018).

[52] T. Tian, Y. Cai, X. Wu, and Z. Wen, Ground states of spin-f Bose-Einstein condensates, SIAM J. Sci. Comput. **42**, B983 (2020).

[53] P. A. Andreev, I. N. Mosaki, and M. I. Trukhanova, Quantum hydrodynamics of the spinor Bose-Einstein condensate at non-zero temperatures, Phys. Fluids **33**, 067108 (2021).

[54] S. Sriburadet, Y.-T. Shih, B.-W. Jeng, C.-H Hsueh, and C.-S. Chien, A numerical scheme for the ground state of rotating spin-1 Bose-Einstein condensates, Sci. Rep. **11**, 22801 (2021).

[55] H.-Y. Zhang, M. Jain, and M. A. Amin, Polarized vector oscillons, Phys. Rev. D **105**, 096037 (2022).

[56] C. de Rham, G. Gabadadze, and A. J. Tolley, Resummation of massive gravity, Phys. Rev. Lett. **106**, 231101 (2011).

[57] S. F. Hassan and R. A. Rosen, Resolving the ghost problem in non-linear massive gravity, Phys. Rev. Lett. **108**, 041101 (2012).

[58] S. F. Hassan, R. A. Rosen, and A. Schmidt-May, Ghost-free massive gravity with a general reference metric, J. High Energy Phys. 02 (2012) 026.

[59] S. F. Hassan and R. A. Rosen, Bimetric gravity from ghost-free massive gravity, J. High Energy Phys. 02 (2012) 126.

[60] K. Hinterbichler, Theoretical aspects of massive gravity, Rev. Mod. Phys. **84**, 671 (2012).

[61] C. de Rham, Massive gravity, Living Rev. Relativ. **17**, 7 (2014).

[62] A. Schmidt-May and M. von Strauss, Recent developments in bimetric theory, J. Phys. A: Math. Theor. **49**, 183001 (2016).

[63] E. Babichev, L. Marzola, M. Raidal, A. Schmidt-May, F. Urban, H. Veermäe, and M. von Strauss, Heavy spin-2 dark matter, J. Cosmol. Astropart. Phys. 09 (2016) 016.

[64] I. D. Gialamas and K. Tamvakis, Bimetric-affine quadratic gravity, Phys. Rev. D **107**, 104012 (2023).

[65] N. Goldman, G. Juzeliūnas, P. Öhberg, and I. B. Spielman, Light-induced gauge fields for ultracold atoms, Rep. Prog. Phys. **77**, 126401 (2014).

[66] H. Zhai, Degenerate quantum gases with spin-orbit coupling: A review, Rep. Prog. Phys. **78**, 026001 (2015).

[67] L. M. Symes, R. I. McLachlan, and P. B. Blakie, Efficient and accurate methods for solving the time-dependent spin-1 Gross-Pitaevskii equation, Phys. Rev. E **93**, 053309 (2016).

[68] L. M. Symes and P. B. Blakie, Solving the spin-2 Gross-Pitaevskii equation using exact nonlinear dynamics and symplectic composition, Phys. Rev. E **95**, 013311 (2017).

[69] C. V. Ciobanu, S.-K. Yip, and T.-L. Ho, Phase diagrams of $f = 2$ spinor Bose-Einstein condensates, Phys. Rev. A **61**, 033607 (2000).

[70] B. D. Smith, L. W. Cooke, and L. J. LeBlanc, GPU-accelerated solutions of the nonlinear Schrödinger equation for simulating 2D spinor BECs, Comput. Phys. Commun. **275**, 108314 (2022).

[71] M. Jain and M. A. Amin, i-SPin: An integrator for multicomponent Schrödinger-Poisson systems with self-interactions, J. Cosmol. Astropart. Phys. 04 (2023) 053.

[72] R. van Wageningen, Explicit polynomial expressions for finite rotation operators, Nucl. Phys. **60**, 250 (1964).

[73] Y. Lehrer-Ilamed, On the direct calculations of the representations of the three-dimensional pure rotation group, Math. Proc. Cambridge Philos. Soc. **60**, 61 (1964).

[74] T. L. Curtright, D. B. Fairlie, and C. K. Zachos, A compact formula for rotations as spin matrix polynomials, SIGMA **10**, 084 (2014).

[75] S. Jiang, L. Greengard, and W. Bao, Fast and accurate evaluation of nonlocal Coulomb and dipole-dipole interactions via the nonuniform FFT, SIAM J. Sci. Comput. **36**, B777 (2014).

[76] W. Bao, Q. Tang, and Y. Zhang, Accurate and efficient numerical methods for computing ground states and dynamics of dipolar Bose-Einstein condensates via the nonuniform FFT, Commun. Comput. Phys. **19**, 1141 (2016).

[77] W. Bao, Y. Cai, and H. Wang, Efficient numerical methods for computing ground states and dynamics of dipolar Bose-Einstein condensates, J. Comput. Phys. **229**, 7874 (2010).

[78] X.-F. Zhou, C. Wu, G.-C. Guo, R. Wang, H. Pu, and Z.-W. Zhou, Synthetic Landau levels and spinor vortex matter on a haldane spherical surface with a magnetic monopole, Phys. Rev. Lett. **120**, 130402 (2018).

[79] X. Liu, H. Pu, B. Xiong, W. M. Liu, and J. Gong, Formation and transformation of vector solitons in two-species Bose-Einstein condensates with a tunable interaction, Phys. Rev. A **79**, 013423 (2009).

[80] K. E. Strecker, G. B. Partridge, A. G. Truscott, and R. G. Hulet, Formation and propagation of matter-wave soliton trains, Nature (London) **417**, 150 (2002).

[81] J. H. V. Nguyen, P. Dyke, D. Luo, B. A. Malomed, and R. G. Hulet, Collisions of matter-wave solitons, Nat. Phys. **10**, 918 (2014).

[82] D. Luo, Y. Jin, J. H. V. Nguyen, B. A. Malomed, O. V. Marchukov, V. A. Yurovsky, V. Dunjko, M. Olshanii, and R. G. Hulet, Creation and characterization of matter-wave breathers, Phys. Rev. Lett. **125**, 183902 (2020).

[83] H. Sakaguchi, B. Li, and B. A. Malomed, Creation of two-dimensional composite solitons in spin-orbit-coupled self-attractive Bose-Einstein condensates in free space, Phys. Rev. E **89**, 032920 (2014).

[84] Y.-C. Zhang, Z.-W. Zhou, B. A. Malomed, and H. Pu, Stable solitons in three dimensional free space without the ground state: Self-trapped Bose-Einstein condensates with spin-orbit coupling, Phys. Rev. Lett. **115**, 253902 (2015).

[85] B. Salehian, H.-Y. Zhang, M. A. Amin, D. I. Kaiser, and M. H. Namjoo, Beyond Schrödinger-Poisson: Nonrelativistic effective field theory for scalar dark matter, J. High Energy Phys. (2021) 050.

[86] R. A. Porto, The effective field theorist's approach to gravitational dynamics, Phys. Rep. **633**, 1 (2016).

[87] B. Cashen, A. Aker, and M. Kesden, Gravitomagnetic dynamical friction, Phys. Rev. D **95**, 064014 (2017).

[88] P.-H. Chavanis, Mass-radius relation of Newtonian self-gravitating Bose-Einstein condensates with short-range interactions: I. Analytical results, Phys. Rev. D **84**, 043531 (2011).

[89] P.-H. Chavanis, Collapse of a self-gravitating Bose-Einstein condensate with attractive self-interaction, Phys. Rev. D **94**, 083007 (2016).

[90] M. A. Amin and P. Mocz, Formation, gravitational clustering, and interactions of nonrelativistic solitons in an expanding universe, Phys. Rev. D **100**, 063507 (2019).

[91] P.-H. Chavanis, Jeans instability of dissipative self-gravitating Bose-Einstein condensates with repulsive or attractive self-interaction: Application to dark matter, Universe **6**, 226 (2020).

[92] T. Dawoodbhoy, P. R. Shapiro, and T. Rindler-Daller, Core-envelope haloes in scalar field dark matter with repulsive self-interaction: Fluid dynamics beyond the de Broglie wavelength, Mon. Not. R. Astron. Soc. **506**, 2418 (2021).

[93] P. R. Shapiro, T. Dawoodbhoy, and T. Rindler-Daller, Cosmological structure formation in scalar field dark matter with repulsive self-interaction: The incredible shrinking Jeans mass, Mon. Not. R. Astron. Soc. **509**, 145 (2021).

[94] S. Chakrabarti, B. Dave, K. Dutta, and G. Goswami, Constraints on the mass and self-coupling of ultra-light scalar field dark matter using observational limits on galactic central mass, J. Cosmol. Astropart. Phys. 09 (2022) 074.

[95] P.-H. Chavanis, Maximum mass of relativistic self-gravitating Bose-Einstein condensates with repulsive or attractive $|\varphi|^4$ self-interaction, Phys. Rev. D **107**, 103503 (2022).

[96] P. Mocz *et al.*, Cosmological structure formation and soliton phase transition in fuzzy dark matter with axion self-interactions, Mon. Not. R. Astron. Soc. **521**, 2608 (2023).

[97] D. G. Levkov, A. G. Panin, and I. I. Tkachev, Gravitational Bose-Einstein condensation in the kinetic regime, Phys. Rev. Lett. **121**, 151301 (2018).

[98] B. Eggemeier and J. C. Niemeyer, Formation and mass growth of axion stars in axion miniclusters, Phys. Rev. D **100**, 063528 (2019).

[99] J. Chen, X. Du, E. W. Lentz, D. J. E. Marsh, and J. C. Niemeyer, New insights into the formation and growth of boson stars in dark matter halos, Phys. Rev. D **104**, 083022 (2021).

[100] J. H.-H. Chan, S. Sibiryakov, and W. Xue, Condensation and evaporation of boson stars, arXiv:2207.04057.

[101] M. Jain, M. A. Amin, J. Thomas, and W. Wanichwecharungruang, Kinetic relaxation and Bose-star formation in multicomponent dark matter—I, Phys. Rev. D **108**, 043535 (2023).

[102] J. Chen, X. Du, M. Zhou, A. Benson, and D. J. E. Marsh, Gravitational Bose-Einstein condensation of vector/hidden photon dark matter, Phys. Rev. D **108**, 083021 (2023).

[103] T. Helfer, E. A. Lim, M. A. G. Garcia, and M. A. Amin, Gravitational wave emission from collisions of compact scalar solitons, Phys. Rev. D **99**, 044046 (2019).

[104] N. Sanchis-Gual, J. C. Bustillo, C. Herdeiro, E. Radu, J. A. Font, S. H. W. Leong, and A. Torres-Forné, Impact of the wavelike nature of Proca stars on their gravitational-wave emission, Phys. Rev. D **106**, 124011 (2022).

[105] M. A. Amin, A. J. Long, and E. D. Schiappacasse, Photons from dark photon solitons via parametric resonance, J. Cosmol. Astropart. Phys. 05 (2023) 015.

[106] S. Blanes and P. Moan, Practical symplectic partitioned Runge-Kutta and Runge-Kutta-Nyström methods, J. Comput. Appl. Math. **142**, 313 (2002).